Centro Brasileiro de Pesquisas Físicas

Coordenação de Educação

COTEO

Joaquim de Miranda Telles de Miranda

Entanglement Properties of Ergodic Quantum States

Rio de Janeiro - RJ

July 26, 2023

Joaquim de Miranda Telles de Miranda

Entanglement Properties of Ergodic Quantum States

Dissertação apresentada ao curso de Pós-Graduação em Física do Centro Brasileiro de Pesquisas Físicas, como requisito parcial para a obtenção do Título de mestre em Física.

Orientador:

Tobias Micklitz

July 26, 2023

CBPF
Centro Brasileiro de Pesquisas Físicas
SUBORDINADA AO MCTI

MINISTÉRIO DA CIÊNCIA, TECNOLOGIA E INOVAÇÕES

"ENTANGLEMENT PROPERTIES OF ERGODIC QUANTUM STATES"

JOAQUIM DE MIRANDA TELLES DE MIRANDA

Dissertação de Mestrado em Física apresentada no Centro Brasileiro de Pesquisas Físicas do Ministério da Ciência Tecnologia e Inovação. Fazendo parte da banca examinadora os seguintes professores:

Tobias Micklitz – Orientador/CBPF

Thiago Rodrigues de Oliveira - UFF

Fernando Iemini de Rezende Aguiar – UFF

Rio de Janeiro, 04 de abril de 2023.

Agradecimentos

Agradecimentos e mensagens de carinho não são meu ponto forte. Sendo assim, serei conciso e torço para que todos se sintam abraçados. Um agradecimento especial para:

Minha família e namorada Camila pelo apoio e amor ao longo de todo este trabalho,

Meu orientador Tobias Micklitz por toda a atenção e tudo que me ensinou,

Os amigos que fiz ao longo da minha graduação na UFRJ e mestrado no CBPF,

A CAPES pelo apoio financeiro.

Contents

List of Figures

Resumo

Nessa dissertação nós estudamos propriedades de emaranhamento de estados associados a sistemas quânticos ergódicos. Especificamente, nós desenvolvemos descrições analíticas para a *entanglement entropy*, *relative entropy* e *trace distance* destes estados após uma bipartição do sistema em dois subsistemas. Após revisar resultados conhecidos para a *entanglement entropy* e *relative entropy* nós focamos na *trace distance*, relacionada ao problema de discriminação de estados. Isto é, dado um dentre dois estados quânticos conhecidos ρ e σ, a *trace distance* codifica a melhor probabilidade de sucesso de identificar corretamente o estado dado realizando um experimento otimizado, segundo o teorema Holevo-Helstrom. Além disse, resultados foram obtidos tanto para sistemas ergódicos sem qualquer estrutura, quanto para sistemas que conservam alguma carga localmente. Nós checamos a validade de nossos resultados analíticos através da diagonalização exata de sistemas caóticos, encontrando bom acordo entre cálculos e simulações.

Palavras-chave: Trace Distance, Estados aleatórios, Termalização, Information Scrambling.

Abstract

In this dissertation we study entanglement properties of states associated with ergodic quantum systems. Specifically, we develop analytical descriptions of the entanglement entropy, relative entropy and trace distance of such states upon bi-partitioning of the system into two subsystems. After review of known results for the entanglement entropy and relative entropy we focus on the trace distance, related to the problem of state discrimination. That is, given one of two known quantum states ρ and σ, the trace distance encodes the best success probability of correctly identifying the given state performing an optimally chosen experiment, as stated in the Holevo-Hesltrom theorem. Moreover, results are obtained for both ergodic systems lacking any structure and those which conserve some charge locally. We check the validity of our analytical results against exact diagonalization of chaotic quantum systems, finding good agreement between calculations and simulations.

Keywords:Trace Distance, Random states, Thermalization, Information Scrambling.

Introduction

The entanglement properties of random pure states have been a subject of interest for different areas of physics, ranging from black holes and the information paradox [1, 2] to chaotic quantum dynamics and the characterization of states in the the many-body localization transition [3]. In this dissertation we study entanglement properties of random pure states using three different measures, namely the entanglement entropy (EE), relative entropy (RE) and trace distance (TD). There have been works exploring these entanglement properties in the context of ergodic states lacking any structure (Page states). We here expand to situations in which a locally conserved charge upon bipartition of the system, a scenario recently explored in Ref. [3, 4]. Then we turn to the main interest of the work, the TD. Amongst entanglement properties, the TD is interesting as the main tool in state discrimination, which is important for understanding thermalization. To the best of our knowledge a fully analytical description of the TD property had not, to the best of our knowledge, been developed yet. We will develop this treatment for both Page states and in situations with conservation laws, as well as check all results against exact diagonalization of quantum systems. Our main findings have been made available in the preprint server arxiv.org, to be published in Journal of Physics A: Mathematical and Theoretical [5].

First of all, it is necessary to make clear what is meant by "ergodic states". Ergodic systems in the classical sense are those who, given enough time, span the full phase space available to them, which may or may not have constraints such as energy and momentum conservation. Obviously, given the nature of quantum mechanics and the Heisenberg uncertainty principle, it is not possible to define quantum ergodicity in the same terms. While there is not a precise definition of ergodicity in quantum mechanical systems, a well accepted definition, and one adopted in this work, is that ergodic states are those who follow the eigenstate thermalization hypothesis (ETH) and thermalize to infinite

temperature. The ETH says that: given an isolated quantum system in an arbitrary initial state, it will evolve (thermalize) so to scramble the initial information into extensively many degrees of freedom, such that observables of small (but finite) subsystems will be described by statistical mechanics principles, up to small fluctuations. This is observed in several quantum systems and is a well established concept in condensed matter physics. For a comprehensive review on the ETH the reader can refer to [6]. To be more concrete, for generic ergodic states (i.e. in the middle of the spectrum, not at the edges), we expect the leading order term of the entanglement properties to correspond to an thermal equilibrium density matrix for the canonical ensemble at infinite temperature, i.e. $\rho \approx \mathbb{1}/D$, where $\mathbb{1}$ is the identity matrix and D is the dimension of the Hilbert space available to the system.

As mentioned, plenty of work has already been done when it comes to entanglement properties of quantum ergodic states. In a seminal work, D. Page studied the average bipartite entanglement entropy for fully random states - Page states [7]. The "Page curve" shows that the entanglement entropy of the reduced density matrix of these states is due to a classical and a quantum contribution, the former (leading term) being the thermal entropy of a maximally mixed state - in accordance with the ETH - and the latter (correction term) describes the average information stored in the system. Other works have also studied the relative entropy between the reduced density matrix of the bipartite states [8], as well as the trace distance between them [9].

However, the solution for the trace distance obtained in Ref. [9], while quite illuminating, stumbled upon a difficult combinatorial problem which was solved by restricting to leading terms. As will be discussed properly in later sections, the trace distance has some very useful properties for comparing quantum states which the relative entropy doesn't possess, the main one being that it defines a metric on the space of density matrices. Also, it is intimately related to the optimal probability of discriminating between quantum states. This feature can prove to be of interest in the task of developing robust quantum information storage devices, which rely on the ability to tell states apart to effectively access stored information. Because of this, the description of the TD for random states is a problem of conceptual and practical importance. The development of an exact solution for the trace distance between Page states will be the main and novel result of this work.

Ergodic states following the ETH must have its observables follow, up to leading order, statistical mechanics descriptions. This definition leaves room for small fluctuations to this behaviour which allow these states to describe several chaotic systems. In previous works, including Page's original work [7], the states studied were strictly fully random, Haar distributed vectors in the full Hilbert space associated with a given system. However, closed many-body systems often present more structure than that, given by local conservation laws. Such conservation laws (e.g. energy or charge conservation) impose restrictions that diminish the entanglement spreading over the system, affecting the properties we wish to study in ways that are less understood. Recent works show, for instance, that the entanglement entropy for ergodic states with conserved quantities do not follow the Page curve, but have a correction to the quantum contribution [3]. Thus, another goal of this work is to study the EE and the TD assuming the system presents local conservation laws. Unfortunately, for reasons that will be discussed later, we were not able to extend this discussion to the RE.

Along with the analytical predictions developed, we perform simulations of models that should fit into our assumptions when working with states with and without conservation laws, and verify results via exact diagonalization of ergodic systems. Our focus is on qubit systems, whose Hilbert space is suited for the bipartitions we shall consider, but also are of interest in their own merit, as currently vastly studied systems. For simulating structureless, fully random states, we will use the Majorana SYK model which is known to be thermalizing and displays no local conservation laws [10, 11]. As for a system with an extensively conserved local charge we choose to work with a spin-1/2 Ising chain with longitudinal and transversal fields, a system that is known to be strongly thermalizing for properly chosen field strengths [12, 13, 14], but that conserves energy locally.

The dissertation is structured in the following manner: We begin in chapter 1 by presenting some of the physical concepts that are linked to random states. In Chapter 2 we present the entanglement properties we will study throughout. In Chapter 3 we work on some combinatorial results that will be necessary to evaluate the replica-tricks later. Chapters 4 and 5 are the bulk of the work, where we present the theoretical predictions along with simulation results for states with and without conservation laws. Chapter 4 reviews previous results in the literature concerning the entanglement entropy and the relative entropy, while in Chapter 5 we present novel contributions on the trace distance.

Finally, in Chapter 6 we present the methods employed in the simulation as well as a more comprehensive presentation of the models we worked with.

Chapter 1

Physical Concepts

While ergodic states are of interest on their own, we can make the discussion much richer by exploring some physical concepts directly linked to them. For this purpose, we take a quick chapter to delve into some of those, discussing the thermalization of quantum systems and a its relationship with random matrix theory.

1.1 Eigenstate Thermalization Hypothesis (ETH)

Quantum mechanics is a theory built on the notion of unitary evolution of systems via Schrödinger's equation. Unitary evolution cannot erase information, thus, if we are given an initial state for a closed quantum system, all information regarding that state must be preserved within the system at all times. However, the notion of thermalization of systems is linked to the idea of a system 'forgetting' about its initial state and entering in equilibrium with some 'bath', making possible to describe it with a few parameters such as temperature, chemical potential and etc. How do we conciliate both views?

Even though information is not erased in the evolution of closed quantum systems, it is *scrambled* through the process of decoherence. Through this process, information regarding few-body-operators in the system is spread across all degrees of freedom. This makes it such that knowledge on some initial state is essentially inaccessible as it would require measuring global operators, which is often not feasible [1]. Thus, as we look into a *small* subsystem of the whole closed system it can *appear* thermal, with the rest of the

[1] Here by global operators we mean operators which act non-trivially in a fraction of the system of the order of the whole system. That is, if the system consists of N qubits, a global operators would act as non-identity operators on $k \sim \mathcal{O}(N)$ qubits.

system acting as a large bath. The ETH postulates how this takes place mathematically. By studying the trace distance on later chapters we provide answers to the questions of how small must that subsystem be, and how much the system 'appears' thermal.

The ETH postulates that, given two energy eigenstates $|E_m\rangle$ and $|E_n\rangle$ of a chaotic system, the expectation value of a few-body-operator $\hat{O}$ behaves thermally as

$$\langle E_m|\hat{O}|E_n\rangle = f_{\hat{O}}(E)\delta_{mn} + \Omega^{-1/2}(E)r_{mn}, \tag{1.1}$$

where $f_{\hat{O}}(E)$ is a smooth function of $E = (E_m + E_n)/2$, $\Omega(E) = e^{S(E)}$ is the density matrix of the full system, and the fluctuations are of order $r_{mn} \sim \mathcal{O}(1)$. This is expected to hold for generic non-integrable systems, and breaks down if one considers integrable or many-body localized systems where information scrambling is suppressed. Notably, the above statement says that expectation values of few-body operators appear thermal up to exponentially small fluctuations.

1.1.1 Subsystem ETH

While the ETH provides us gives us plenty insight into the thermalization of quantum systems, another proposition, the subsystem eigenstate thermalization hypothesis [15], considerably strengthens the postulate. This variation postulates that the density matrix of small enough subsystem of a chaotic many-body system appears thermal itself.

Subsystem ETH states that the reduced density matrix $\rho_A^{(m)} = \mathrm{tr}_B\, |E_m\rangle \langle E_m|$ in a sufficiently small subsystem A of a chaotic system, B being the rest of the system, is exponentially close to some universal reduced density matrix $\rho_A(E)$ which depends smoothly on energy E,

$$\frac{1}{2}||\rho_A^{(m)} - \rho_A(E = E_m)||_1 \sim \mathcal{O}[\Omega^{-1/2}(E_m)], \tag{1.2}$$

where $\frac{1}{2}||O||_1 = \frac{1}{2}\,\mathrm{tr}\,\sqrt{O^\dagger O}$. The right hand side above is the trace distance between $\rho_A^{(m)}$ and $\rho_A(E = E_m)$. Moreover, the subsystem ETH also postulates that "off-diagonal" density matrices $\rho_A^{(mn)} = \mathrm{tr}_B\, |E_m\rangle \langle E_n|$ $(E_m \neq E_n)$ are exponentially small,

$$||\rho_A^{(mn)}|| \sim \mathcal{O}[\Omega^{-1/2}(E)]. \tag{1.3}$$

As we develop analytical results for the trace distance in of ergodic states in Chapter

5, we will be concerned in discussing our results in the context of the ETH and subsystem ETH, looking to better grasp the thermalization of closed quantum systems.

1.2 Random Matrix Theory (RMT)

In this brief section we look to present some basic ideas from RMT, a very important tool to understanding thermal systems in the lens of quantum chaos. Originally developed by Wigner for understanding spectra of complex atomic nuclei [16, 17, 18], RMT became a powerful means to understand complex and chaotic quantum systems in general. In particular, it is closed linked to our understanding of thermalization and thermal systems [19].

In order to study complex systems, RMT focuses on understanding statistical properties concerning energy levels and eigenstates of such systems. In order to do so, Wigner had the insight that, if one looks at sufficiently small energy windows for which the density of states is constant, the Hamiltonian looks, in a non fine-tuned basis, like a random matrix. Thus, one can study statistical properties of a system by studying ensembles of random Gaussian-distributed matrices which are constrained simply by symmetries of the system.

As RMT is not the main focus of this dissertation, we quickly review two ensembles of matrices and some statistical properties. Interested readers may refer to Ref. [20] for details. The Gaussian orthogonal ensemble (GOE) and Gaussian unitary ensemble (GUE) can are drawn from the distribution:

$$P(\hat{H}) \propto \exp\left[-\frac{\beta}{2a^2}\,\mathrm{tr}\left(\hat{H}^2\right)\right], \tag{1.4}$$

where for the GOE $\beta = 1$ and $H_{ij} = H_{ji}$ with real elements and for the GUE $\beta = 2$ and $H_{ij} = H^*_{ji}$ with complex elements, while a defines the energy scale of the system. The GOE and GUE describe systems with and without time-reversal symmetry respectively, and we restrict to them in this exposition. Notably, the choices above for our ensembles are very natural. For one, the GOE and GUE are invariant under orthogonal and unitary transformations respectively. Also, as sums of a large number of independent contributions, the Gaussian distribution satisfies the central limit theorem.

In particular, we can use these ensembles to define our notion of ergodicity of quantum

systems. We thus call ergodic systems whose eigenfunctions $|\psi\rangle = \sum_n \psi_n |n\rangle$ obey Porter-Thomas distributions,

$$P_{GOE}(y) = \frac{1}{\sqrt{2\pi y}} e^{-\frac{y}{2}}, \qquad P_{GUE}(y) = e^{-y}, \tag{1.5}$$

with $y = D|\psi_n|^2$, D being the dimension of the Hilbert space associated with the system.

Finally, we conclude by pointing the close relation between the ETH and RMT. Namely, it can be shown that the predictions for expectation values of observables using the ETH ansatz and RMT tools coincide if we look into narrow energy windows [19]. This observation allows us to use RMT to stablish the paradigms for ergodic/thermal systems.

Chapter 2

Entanglement Properties

In this chapter we give a presentation of the entanglement entropy, relative entropy and trace distance, which will be the objects of study of this work. We are interested in evaluating these properties in states of bi-partitioned systems. Consider a D-dimensional Hilbert space associated to a given quantum system. We perform an entanglement-cut bi-partitioning the Hilbert space into two of dimensions D_A and D_B such that $D_A D_B = D$, and each of those is associated with subsystems A and B of the total system. In our case, for instance, we are interested in a N qubit system whose Hilbert space is of dimension $D = 2^N$ and the subsystems consist in two sets of N_A and N_B of the qubits ($N_A+N_B = N$), which we call subsystems A and B, respectively. We work with states on the subsystem A, without loss of generality, i.e. we 'trace out' subsystem B.

2.1 Entanglement Entropy (EE)

The entanglement entropy (or von Neumann entropy) is a generalization to quantum mechanics of Shannon's entropy for classical probability distributions, and is a standard measure in quantum information theory. Within the context of quantum mechanics, the EE measures whether a given density matrix corresponds to a mixed state or a pure state. It's definition is:

$$S(\rho) = -\operatorname{tr}(\rho \ln \rho) = -\sum_i \lambda_i \ln \lambda_i, \tag{2.1}$$

where λ_i are the eigenvalues of ρ.

Some of the properties of the EE relevant to this work are (one can refer to [21] for proofs):

1. The entropy is non-negative. The entropy is zero if and only if the state is pure.

2. In a D-dimensional Hilbert space the entropy is at most $\ln D$. The entropy is equal to $\ln D$ if and only if the system is in the completely mixed state $\mathbb{1}/D$.

The above properties justify the employment of the EE as a measure of purity.

However, the EE of bipartite systems has a different interpretation, as a measure of entanglement between the partitions of the system. This can be motivated noting that the reduced density matrix of a composite system AB which is unentangled corresponds to a pure state:

$$\rho_A = \mathrm{tr}_B\, \rho_{AB} = \mathrm{tr}_B[|\psi_A\rangle\, |\phi_B\rangle][\langle\phi_B|\, \langle\psi_A|] = |\psi_A\rangle\, \langle\psi_A|\,, \tag{2.2}$$

and according to the properties listed above, its EE is zero in that case. If the system is entangled that is not the case and the EE will be finite. Therefore, one can obtain information on the degree of entanglement between partitions of the system through the EE.

2.2 Relative Entropy (RE)

The relative entropy is another useful tool from quantum information theory. It is a measure of distinguishability of two states, defined as:

$$S(\rho||\sigma) = \mathrm{tr}(\rho \log \rho) - \mathrm{tr}(\rho \log \sigma), \tag{2.3}$$

with the property:

$$S(\rho||\sigma) \geq 0, \tag{2.4}$$

with equality if and only if $\rho = \sigma$ (again we defer all proofs in this section to [21]).

The RE has its flaws however. For one, it is not bounded, being defined to be $+\infty$ if the kernel of σ intersects with the support of ρ, that is, if:

$$\ker(\sigma) \cup \mathrm{supp}(\rho) \neq 0, \tag{2.5}$$

and it is finite otherwise. Unfortunately this is a problem that presents itself in this work.

As we deal with bipartitions of systems with locally conserved charges, we will evaluate the entanglement properties in subsystem A. If this subsystem' dimension is more than half of the original system's (i.e. $D_A > D/2$), we necessarily have the situation above, and the RE is infinite. We will show that this is the case in Chapter 6. Also, the RE is not a proper *metric* in the space of density matrices, and therefore does not define robust tool for measuring how different two given states are. This is readily seen from the fact that the RE is not symmetric in its inputs.

Although the RE is an imperfect tool for state distinguishability purposes, it is still a very useful one. One of its advantages is that it is easily evaluated compared to other measures that do define a metric (such as the trace distance below, for instance). Moreover, it bounds the trace distance, giving insight in state discrimination via Pinsker's inequality, which will be presented shortly. Because of that it has been more consistently explored in the literature.

2.3 Trace Distance (TD)

Suppose we are given one of two known quantum states ρ and σ, what is the optimal probability of correctly identifying the state? This is a challenging problem, studied in depth solely in the scenario of two state discrimination, see e.g. [22] for a review. The answer to the question is given by the Holevo-Helstrom theorem, which states that the best success probability is encoded in the Schatten 1- or trace-distance as

$$P_{\rho\sigma} = \frac{1}{2} + \frac{1}{2} D_1(\rho, \sigma). \tag{2.6}$$

General Schatten n-distances are defined as:

$$D_n(\rho, \sigma) \equiv \frac{1}{2^{1/n}} ||\rho - \sigma||_n, \tag{2.7}$$

where the n-norm of a matrix Λ is determined by its singular values σ_i as:

$$||A||_n = \left(\sum_i \sigma_i^n \right)^{1/n}. \tag{2.8}$$

The trace-distance also proves to be a more robust tool for evaluating how 'distant'

two given states are. For instance, it does define a metric in the space of density operators, meaning that it obeys the first three of the following relations (as before, proofs can be found in [21]):

1. $D(\rho, \sigma) \geq 0$ and equality holds if and only if $\rho = \sigma$.

2. $D(\rho, \sigma) = D(\sigma, \rho)$, i.e. it is symmetric in its inputs.

3. It obeys the triangle inequality: $D(\rho, \sigma) \leq D(\rho, \tau) + D(\tau, \sigma)$.

4. $D(\rho, \sigma) \leq 1$ with equality if ρ is orthogonal to σ, i.e. if $\mathrm{tr}(\rho\sigma) = 0$.

5. $D(\rho_A, \sigma_A) \leq D(\rho_{AB}, \sigma_{AB})$.

Therefore, it is a proper tool to measure whether two quantum states are 'close' to each other. It can be shown from their definition that the other Schatten distances satisfy the first three properties above, defining themselves metrics, with the TD being of more interest among the others due to the Holevo-Helstrom theorem.

Finally, the trace distance is bounded by the relative entropy as stated in Pinsker's inequality [23, 24]:

$$\frac{1}{2} D_1(\rho, \sigma)^2 \leq S(\rho||\sigma), \tag{2.9}$$

to be checked later. While there are other properties bounding the trace distance (e.g. the fidelity the via Fuchs-van de Graaf inequality [21]), we here restrict to Pinsker's inequality since we develop results for both the trace distance and the relative entropy.

Chapter 3

Noncrossing Partitions

In the next chapters we are concerned with deriving the analytical equations that describe the entanglement properties discussed in the previous chapter for ergodic systems. We will employ replica tricks for our calculations and, as will be seen later, the employment of this technique will lead to combinatorial problems. Therefore it is important to devote a section to establish the tools that will be used in solving these combinatorial problems once and for all.

The central object in our combinatorial problems are noncrossing partitions and we briefly review the key concepts. Given a set of n numbers $[n] \coloneqq 1, 2, ..., n$, a partition is a family of non-empty disjoint sets $B_1, B_2, ..., B_k$ of elements of the set $[n]$, which we call blocks, whose union is the original set. A partition is noncrossing if, given four elements $1 \leq a < b < c < d \leq n$, such that a and c are in the same block and b and d are in the same block, then the two blocks coincide. We can best represent what was said up to here with the aid of diagrams: Figure 3.1 provides examples of partitions of a set of n objects that are crossing and noncrossing. With the use of these diagrams it is easy to see the reason behind the name 'noncrossing partitions': in a linear graphical representation, the lines used to identify blocks never cross for these partitions.

For our purposes, we are interested in counting the number of noncrossing partitions with a fixed number of blocks and set of elements. There are two concepts that are useful for this purpose: Kreweras numbers and Narayana numbers. Kreweras numbers count how many noncrossing partitions with specified block sizes there are. Narayana numbers count noncrossing partitions with a fixed number of blocks. In the sections below are concerned with both of these, as well as, with a generalization of the latter that is needed

Figure 3.1: Examples of two partitions for $n = 8$ elements, given by their graphical representation. Each block is a grouping of elements represented by the lines connecting them, and no lines linked to a given element mean that the block is the element itself. In the left we have 5 blocks: $B_1 = 1, 2$, $B_2 = 3, 6$, $B_3 = 4, 5$, $B_4 = 7$ and $B_5 = 8$. In the right we have 4 blocks: $B_1 = 1, 3$, $B_2 = 2, 4, 7$, $B_3 = 5, 6$ and $B_4 = 8$. The partition in the left is noncrossing, while the one in the right is not.

in later chapters.

3.1 Kreweras Numbers

Kreweras numbers are our starting point for establishing the needed combinatorial concepts. As mentioned before, it counts the number of noncrossing partitions with fixed block sizes. Given the number n of elements in the set we wish to partition, we can denote the set $\Lambda_n = (1^{\lambda_1}, 2^{\lambda_2}, ..., n^{\lambda_n})$ of all partitions with λ_n blocks of n elements. The size of the set of partitions is then the Kreweras number $\mathrm{Krew}(\Lambda_n)$, given by [25, 26]:

$$\mathrm{Krew}(\Lambda_n) = \frac{1}{n+1}\binom{n+1}{\lambda_1, \lambda_2, ..., \lambda_n}, \tag{3.1}$$

where

$$\binom{n}{\lambda_1, \lambda_2, ..., \lambda_n} := \frac{n!}{\lambda_1!\lambda_2! \cdots \lambda_n!(n - \sum_i \lambda_i)!}, \tag{3.2}$$

with the constraint $\sum_i \lambda_i \leq n$, i.e. the number of partitions is at most the number of elements in the set.

Our interest in Kreweras numbers is mainly as a stepping stone in the calculation of other combinatorial result. As the proof above is rather involved and this result is not the focus of the present work, we ask interested readers to consult the original works.

3.2 Narayana Numbers

Narayana numbers count the number of noncrossing partitions with a given number of blocks. Therefore, we can readily see their connection with Kreweras numbers. That is,

the number of noncrossing partitions of a set of n elements into k block is given by the Narayana number:

$$N(n,k) = \sum_{\substack{\Lambda_n \\ l(\Lambda_n)=k}} \mathrm{Krew}(\Lambda_n), \tag{3.3}$$

where $l(\Lambda_n) = \sum_i \lambda_i$ is the number of blocks in the partition Λ_n, as defined for the Kreweras numbers above. This section is concerned with evaluating the sum above.

Substituting the expression for Kreweras numbers we obtain:

$$N(n,k) = \sum_{\substack{\Lambda_n \\ l(\Lambda_n)=k}} \frac{1}{n+1}\binom{n+1}{\lambda_1, \lambda_2, ..., \lambda_n} = \sum_{\substack{\Lambda_n \\ l(\Lambda_n)=k}} \frac{n!}{\lambda_1!\lambda_2! \cdots \lambda_n!(n+1-k)!}. \tag{3.4}$$

This can be put in a more useful form if we take the summations over the $\{\lambda_i\}$ going to infinity and express the constraints as δ-functions:

$$N(n,k) = \sum_{\lambda_1=0}^{\infty}\sum_{\lambda_2=0}^{\infty}\cdots\sum_{\lambda_n=0}^{\infty} \frac{n!}{(n-k+1)!}\frac{1}{\lambda_1!\lambda_2!...\lambda_n!}\delta_{\sum_i \lambda_i,k}\delta_{\sum_i i\lambda_i,n}, \tag{3.5}$$

where the first δ-function fixes the number of blocks and the second the total number of elements. Since n and k are fixed we can take the first fraction out of the summations. We can also write the delta-functions as integrals using the identity:

$$\delta_{x,n} = \frac{1}{2\pi}\int_0^{2\pi} e^{i(x-n)\phi}d\phi = \int_0^1 e^{2\pi i(x-n)\theta}d\theta. \tag{3.6}$$

Thus

$$\begin{aligned} N(n,k) &= \frac{n!}{(n-k+1)!}\int_0^1 ds \int_0^1 dt \sum_{\lambda_1=0}^{\infty}\cdots\sum_{\lambda_n=0}^{\infty}\frac{1}{\lambda_1!...\lambda_n!}e^{2\pi i(\lambda_1+...+\lambda_n-k)s}e^{2\pi i(\lambda_1+...+n\lambda_n-n)t} \\ &= \frac{n!}{(n-k+1)!}\int_0^1 ds \int_0^1 dt \left[\sum_{\lambda_1=0}^{\infty}\frac{e^{2\pi i(s+t)\lambda_1}}{\lambda_1!}\cdots\sum_{\lambda_n=0}^{\infty}\frac{e^{2\pi i(s+nt)\lambda_n}}{\lambda_n!}\right]e^{-2\pi iks}e^{-2\pi int}. \end{aligned} \tag{3.7}$$

Using

$$e^x = \sum_{n=0}^{\infty}\frac{x^n}{n!}, \tag{3.8}$$

we get

$$\begin{aligned} N(n,k) &= \frac{n!}{(n-k+1)!}\int_0^1 ds \int_0^1 dt \Big(e^{e^{2\pi i(s+t)}} e^{e^{2\pi i(s+2t)}} ... e^{e^{2\pi i(s+nt)}} \Big) e^{-2\pi iks} e^{-2\pi int} \\ &= \frac{n!}{(n-k+1)!}\int_0^1 ds \int_0^1 dt \exp\Big(e^{2\pi is} e^{2\pi it} + ... + e^{2\pi is} e^{2\pi int} \Big) e^{-2\pi iks} e^{-2\pi int} \\ &= \frac{n!}{(n-k+1)!}\int_0^1 ds \int_0^1 dt \exp\Big(e^{2\pi is} \Big[e^{2\pi it} + e^{2\pi i2t} + ... + e^{2\pi int} \Big] \Big) e^{-2\pi iks} e^{-2\pi int}. \end{aligned} \tag{3.9}$$

Now we extend the integrals to the complex plane, making variable changes that cast them into contour integrals over a circle of radius 1 centered at the origin

$$\begin{aligned} z(s) &= e^{2\pi is}, \qquad dz = 2\pi i e^{2\pi is} ds, \qquad ds = \frac{dz}{2\pi iz}, \\ w(t) &= e^{2\pi it}, \qquad dw = 2\pi i e^{2\pi it} dt, \qquad dt = \frac{dw}{2\pi iw}. \end{aligned} \tag{3.10}$$

We can now write

$$\begin{aligned} N(n,k) &= \frac{n!}{(n-k+1)!}\oint \frac{dz}{2\pi iz}\oint \frac{dw}{2\pi iw} \exp\big(z[w + w^2 + ... + w^n] \big) z^{-k} w^{-n} \\ &= \frac{n!}{(n-k+1)!}\oint \frac{dz}{2\pi i}\oint \frac{dw}{2\pi i} \frac{e^{z(w+w^2+...+w^n)}}{z^{k+1} w^{n+1}}. \end{aligned} \tag{3.11}$$

Now, the exponentials are analytical over the complex plane, so we can evaluate the expression above straightforwardly through the residue theorem. In both integrals there are singularities at the origin, with the order of the poles given by the powers of the dividends. We have

$$\begin{aligned} N(n,k) &= \frac{n!}{(n-k+1)!}\oint \frac{dw}{2\pi i}\frac{1}{2\pi i} 2\pi i \frac{1}{k!}\left[\partial_z^k \left(z^{k+1} \frac{e^{z(w+w^2+...+w^n)}}{z^{k+1} w^{n+1}} \right) \right]\Bigg|_{z=0} \\ &= \frac{n!}{(n-k+1)!k!}\oint \frac{dw}{2\pi i} \frac{(w + w^2 + ... + w^n)^k}{w^{n+1}} \\ &= \frac{n!}{(n-k+1)!k!}\frac{1}{2\pi i} 2\pi i \frac{1}{n!}\left[\partial_w^n \left(w^{n+1} \frac{(w + w^2 + ... + w^n)^k}{w^{n+1}} \right) \right]\Bigg|_{w=0} \\ &= \frac{1}{k!(n-k+1)!}\left[\partial_w^n (w + w^2 + ... + w^n)^k \right]\Bigg|_{w=0}. \end{aligned} \tag{3.12}$$

The only term in the sum that does not go to zero after the derivatives and the limit $w = 0$ is the power w^n. Since the sum goes beyond this through w^{nk}, we can extend the

sum to infinity as

$$\begin{aligned} N(n,k) &= \frac{1}{k!(n-k+1)!}\left[\partial_w^n (w+w^2+...+w^n)^k\right]\Big|_{w=0} \\ &= \frac{1}{k!(n-k+1)!}\left[\partial_w^n \left(\sum_{j=0}^{\infty} w^j - 1\right)^k\right]\Big|_{w=0}. \end{aligned} \tag{3.13}$$

Using the geometric series (since we can take $|w|<1$ as we will later make $w=0$)

$$\sum_{j=0}^{\infty} x^j = \frac{1}{1-x}, \tag{3.14}$$

we get

$$N(n,k) = \frac{1}{k!(n-k+1)!}\left[\partial_w^n \left(\frac{1}{1-w}-1\right)^k\right]\Big|_{w=0} = \frac{1}{k!(n-k+1)!}\left[\partial_w^n \left(\frac{w}{1-w}\right)^k\right]\Big|_{w=0}. \tag{3.15}$$

By taking derivatives of the geometric series' expression we arrive at the relation

$$\frac{1}{(1-x)^r} = \frac{1}{(r-1)!}\sum_{j=r-1}^{\infty}\frac{j!}{(j-r+1)!}x^{j-r+1}. \tag{3.16}$$

Then

$$\begin{aligned} N(n,k) &= \frac{1}{k!(n-k+1)!}\left[\partial_w^n \left(w^k \frac{1}{(k-1)!}\sum_{j=k-1}^{\infty}\frac{j!}{(j-k+1)!}w^{j-k+1}\right)\right]\Big|_{w=0} \\ &= \frac{1}{k!(k-1)!(n-k+1)!}\left[\partial_w^n \left(\sum_{j=k-1}^{\infty}\frac{j!}{(j-k+1)!}w^{j+1}\right)\right]\Big|_{w=0}. \end{aligned} \tag{3.17}$$

After taking $w=0$ the only power that survives the derivative is the the one with $n=j+1$. Since $\partial_w^n w^n = n!$, we have

$$\begin{aligned} N(n,k) &= \frac{1}{k!(k-1)!(n-k+1)!}\sum_{j=k-1}^{\infty}\frac{j!(j+1)!}{(j-k+1)!}\delta_{j+1,n} \\ &= \frac{1}{k!(k-1)!(n-k+1)!}\frac{(n-1)!n!}{(n-k)!} = \frac{n!}{k!(n-k)!}\frac{1}{n}\frac{n!}{(k-1)!(n-k+1)!} \\ &= \frac{1}{n}\binom{n}{k}\binom{n}{k-1}. \end{aligned} \tag{3.18}$$

The expression above is the one we were searching for.

3.3 Narayana Numbers Variant

Another concept that will prove itself useful later is a variant of Narayana numbers in which we take into account only blocks with an even number of elements. We can translate that request to Kreweras numbers as

$$\text{Krew}(\Lambda^e_{2n}) = \frac{n!}{\lambda_2!\lambda_4!...\lambda_{2n}!(2n - l(\Lambda^e_{2n}) + 1)!} \quad ; \quad l(\Lambda^e_{2n}) = k = \sum_{i=2,4...}^{2n} \lambda_i \tag{3.19}$$

where $\Lambda^e_{2n} = (2^{\lambda_2}, 4^{\lambda_4}, ..., 2n^{\lambda_{2n}})$. Then, summing over Λ^e_{2n} we get a variant version of Narayana numbers in which we take into account only even-element blocks,

$$N_e(2n, k) = \sum_{\substack{\Lambda^e_{2n} \\ l(\Lambda^e_{2n})=k}} Krew(\Lambda^e_{2n}). \tag{3.20}$$

From there onwards the calculation mirrors exactly the one in the previous sections. Sparing readers from a step-by-step redoing of those, we simply write the result as

$$N_e(2n, k) = \frac{1}{n}\binom{n}{k}\binom{2n}{k-1}. \tag{3.21}$$

Now, taking $2n \to n$ so that the fact that n is even is implicit, we arrive at

$$N_e(n, k) = \frac{2}{n}\binom{n/2}{k}\binom{n}{k-1}. \tag{3.22}$$

This new combinatorial object counts the number of noncrossing partitions of a set of n objects (assumed to be an even-number), into k blocks containing an even number of elements. For reasons to be made clear in the following sections, we will need this variant when evaluating the trace distance of ergodic states.

Chapter 4

Literature Review

In this chapter we review and reproduce some of already established results in the literature concerning the entanglement properties of ergodic states. We start by presenting the two sets of states we will work with, and then move to the proper calculations. Firstly, we reproduce Page's seminal result for the entanglement entropy of states which carry his name [7]. Expanding upon this result, we look to evaluate the EE for states with local conservation laws, reproducing recent results of Ref. [3]. However, here we employ a different formalism, choosing instead to borrow from Ref. [4] to develop our results, both in this chapter and in the next one, when dealing with conservation laws. This choice is due to Ref. [4] using a more general approach, whereas the treatment in Ref. [3] is more specific to a fixed system. Finally, we conclude with the calculation of the relative entropy for Page states, reproducing previous results of Ref. [8]. We were not able, however, develop results for the RE of states with local conservations laws, and discuss why.

4.1 Page states and eigenstates of systems with conservation laws

Having established the entanglement properties we wish to study as well as some useful combinatoric tools in the previous two chapters, we now look to delve into the task of developing analytical descriptions for the entanglement properties in the specific context of ergodic states. We will work with two different set of states: Page states, which are uniformly distributed over the system's Hilbert space, and states with conservation laws, which locally conserve some extensive charge upon system bipartitioning. We thus take

this brief section to define both sets of states.

We focus, without much loss of generality, on bipartite qubit systems, i.e. a collection of N two-level systems. This approach makes the formalism tailor-made for practical problems. Therefore we are dealing with states in a $D = 2^N$ dimensional Fock space, N being the number of qubits in the system. The entanglement cut $|n\rangle = |a\rangle \otimes |b\rangle$ divides the set of qubits in two subsystems, with subspaces of dimensions $D_A = 2^{N_A}$ and $D_B = 2^{N_B}$ respectively, where N_A is the number of qubits in the so-called fist section of the 'chain' and N_B the number of qubits in the second half. We note that, since $N = N_A + N_B$, $D = D_A D_B$. We can write a general state of the Hilbert space of interest as

$$|\psi\rangle = \sum_{a,b} \psi_{ab} \, |a, b\rangle \, , \tag{4.1}$$

where $|a, b\rangle \equiv |a\rangle \otimes |b\rangle$ is a basis of the Hilbert space formed as the tensor product of orthonormal bases $\{|a\rangle\}$ and $\{|b\rangle\}$ for subsystems A and B, respectively. Associated with the general state above is the pure-state density matrix

$$\rho = |\psi\rangle \langle\psi| = \sum_{a,b} \sum_{a',b'} \psi_{ab} \bar{\psi}_{a'b'} \, |a, b\rangle \langle a', b'| \, . \tag{4.2}$$

The reduced density matrices associated with the subsystems A and B established by the entanglement cut are found by tracing over subsystem B, respectively, A

$$\rho_A = \mathrm{tr}_B \, \rho = \sum_{b''} \langle b''| \left[\sum_{a,b} \sum_{a',b'} \psi_{ab} \bar{\psi}_{a'b'} \, |a, b\rangle \langle a', b'| \right] |b''\rangle = \sum_{a,a'} \sum_{b''} \psi_{ab''} \bar{\psi}_{a'b''} \, |a\rangle \langle a'| \, , \tag{4.3}$$

$$\rho_B = \mathrm{tr}_A \, \rho = \sum_{a''} \langle a''| \left[\sum_{a,b} \sum_{a',b'} \psi_{ab} \bar{\psi}_{a'b'} \, |a, b\rangle \langle a', b'| \right] |a''\rangle = \sum_{b,b'} \sum_{a''} \psi_{a''b} \bar{\psi}_{a''b'} \, |b\rangle \langle b'| \, . \tag{4.4}$$

We are focusing our analysis on the N_A-bit sector, that is, we want to study how entanglement properties respond as we trace-out N_B qubits. The larger N_B is, the less information about the system we have access to. Up to here we have looked at the bi-partition structure, which concern both sets, now let us see what defines each one.

For Page states, we set the amplitudes ψ_{ab} of our random pure state to be Gaussian distributed complex numbers, with zero mean and variance

. (4.5)

States $|\psi\rangle$ thus describe infinite temperature thermal states of generic chaotic systems lacking any structure. Also, when using (4.5) we assume that the effects of the normalization constraint in states $|\psi\rangle$ are negligible on average for reasonably large systems, $D \gg 1$. This shortly defines Page states.

Now we move to states with local conservation laws. While Page states are certainly important and interesting on their own, we may want eventually to extend our knowledge to more 'physical' states. We can get closer to those by introducing some structure to our system in the form of conservation laws, more specifically by requiring our states to locally conserve some extensive charge upon bipartition of the system.

Let us suppose the system has a locally conserved quantity Q upon bipartition of the system and we wish to investigate how this affects the entanglement properties. More specifically, we consider a single, extensive conserved scalar operator $\hat{Q}$ that is subsystem additive. That is, a partition of the system in subsystems A and B implies a decomposition $\hat{Q} = \hat{Q}_A + \hat{Q}_B$, such that eigenstates $\hat{Q}\,|n\rangle = Q(n)\,|n\rangle$ can be labelled $|n\rangle = |a, b\rangle$ with $\hat{Q}_A\,|a, b\rangle = Q_A(a)\,|a, b\rangle$ and $\hat{Q}_B\,|a, b\rangle = Q_B(b)\,|a, b\rangle$ satisfying $Q(n) = Q_A(a) + Q_B(b)$. We refer to the locally conserved quantity Q as a 'charge', but it is clear from its definition that it can be e.g. the system's particle number, uni-axial magnetization or energy. We must add this restriction into the general amplitude in (4.5) by defining its second moment as:

$$\langle \psi_{ab} \bar{\psi}_{a'b'} \rangle = \frac{\delta_{aa'}\delta_{bb'}}{F(Q)} \delta_{Q_A(a)+Q_B(b),Q}, \tag{4.6}$$

where $F(Q)$ is the spectral distribution of $\hat{Q}$:

$$F(Q) \equiv D\Omega(Q) = \sum_{a,b} \delta_{Q_A(a)+Q_B(b),Q}, \tag{4.7}$$

and $\Omega(Q)$ is the unit normalized spectral density. Essentially, $F(Q)$ is the dimension of the subspace of the Hilbert space which follows our conservation requirement. For a more in depth discussion on this we refer to Appendix A.

This concludes the presentation. When working with Page states it will suffice to turn to (4.5), while for states with local conservation laws we use (4.6). We now move to calculate entanglement properties using the definitions above.

4.2 Entanglement Entropy (EE) - Page states

To evaluate the EE for random states we employ the replica-trick:

$$S(\rho_A) = -\partial_r M_r|_{r=1} \tag{4.8}$$

with the moments of the reduced density matrix given by $M_r \equiv \langle \mathrm{tr}_A(\rho_A^r)\rangle$. This stems from:

$$-\partial_r \left\langle \mathrm{tr}_A(\rho_A^r)\right\rangle |_{r=1} = -\left\langle \mathrm{tr}_A(\partial_r e^{r\ln\rho_A})\right\rangle\Big|_{r=1} = -\left\langle \mathrm{tr}_A(e^{r\ln\rho_A}\ln\rho_A)\right\rangle\Big|_{r=1} \tag{4.9}$$

$$= -\left\langle \mathrm{tr}_A(\rho_A \ln\rho_A)\right\rangle \equiv S_A(\rho_A), \tag{4.10}$$

and we will drop the index on the EE as it is clear from the index in the density matrix that it is evaluated on subsystem's A Hilbert space, i.e. $S_A(\rho_A) \to S(\rho_A)$.

Therefore, we begin by evaluating the moments. Remembering the most general reduced density matrix in (4.2), we have that:

$$\begin{aligned}\mathrm{tr}_A(\rho_A^r) &= \sum_a \langle a| \left(\sum_{a^1,a'^1}\sum_{b^1}\psi_{a^1b^1}\bar{\psi}_{a'^1b^1}\left|a^1\right\rangle\left\langle a'^1\right|\right)\cdots\left(\sum_{a^r,a'^r}\sum_{b^r}\psi_{a^rb^r}\bar{\psi}_{a'^rb^r}\left|a^r\right\rangle\left\langle a'^r\right|\right)|a\rangle \\ &= \sum_{\{a^i\}}\sum_{\{b^i\}}\psi_{a^1b^1}\bar{\psi}_{a^2b^1}\psi_{a^2b^2}\bar{\psi}_{a^3b^2}\cdots\psi_{a^rb^r}\bar{\psi}_{a^1b^r},\end{aligned} \tag{4.11}$$

yielding,

$$M_r = \langle \mathrm{tr}_A(\rho_A^r)\rangle = \sum_{\{a^i\}}\sum_{\{b^i\}}\langle\psi_{a^1b^1}\bar{\psi}_{a^2b^1}\psi_{a^2b^2}\bar{\psi}_{a^3b^2}\cdots\psi_{a^rb^r}\bar{\psi}_{a^1b^r}\rangle. \tag{4.12}$$

Let us try to make sense of the average above. The amplitudes, as zero-mean Gaussian-distributed variables, if let to fluctuate by themselves yield a null contribution, in what is called a random phase cancellation. Thus, we must look at contributions stemming from larger moments for the non-zero contribution to the average. Because we are dealing with Gaussian variables, we can restrict ourselves to second moments, i.e. $\langle\psi_{ab}\bar{\psi}_{a'b'}\rangle$. Thus, the non-zero contributions to the sum come from coupling two of the many ψ_{ab} and $\bar{\psi}_{a'b'}$ and averaging over them together. In doing this, we make use of (4.5), which equates the indices of the amplitudes via a delta function and introduces a factor $1/D$. Then, after coupling each of the $2r$ amplitudes we are left with an overall factor D^{-r}, as well as

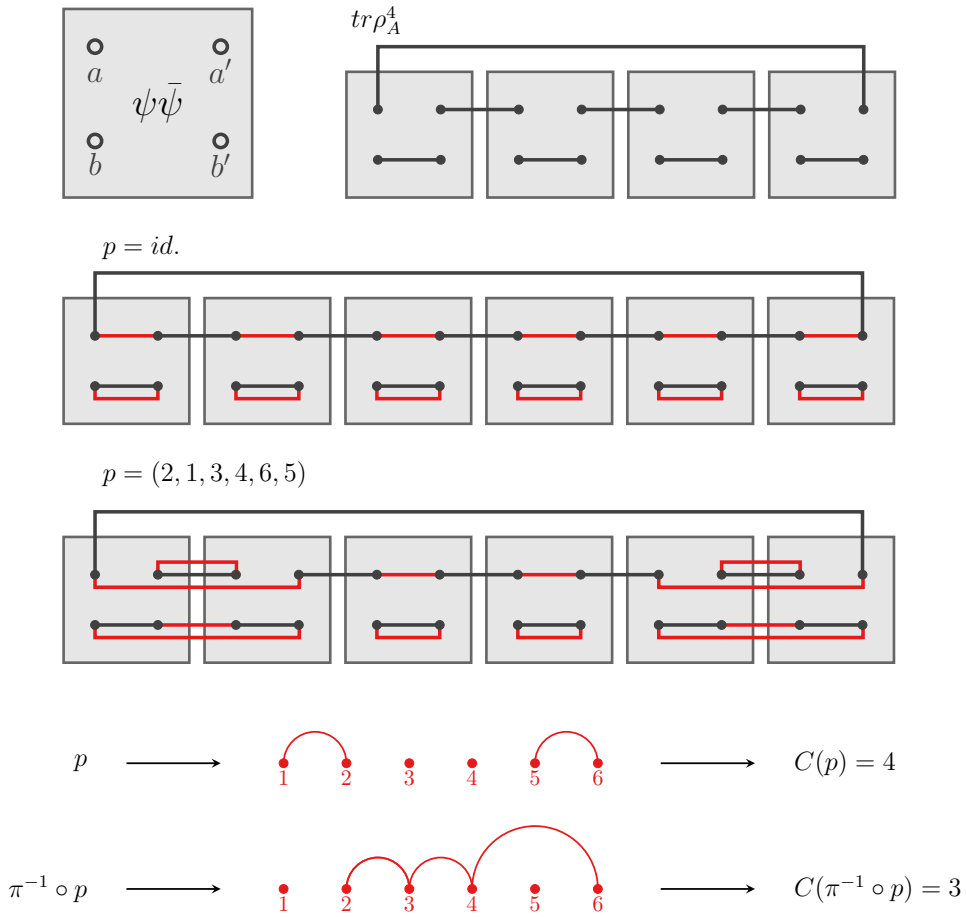

Figure 4.1: Top left: graphic representation of the tensor amplitude $\psi_{ab}\bar{\psi}_{a'b'}$. Top right: contraction of indices defining $\mathrm{tr}_A(\rho_A^4)$. Bellow: averaging enforces pairwise equality of indices a, b, a', b' in tensor products $\left\langle ...\psi_{ab}...\bar{\psi}_{a'b'}...\right\rangle$, as indicated by red lines, in this case for the identity permutation $p = id.$ acting on $\mathrm{tr}_A(\rho_A^6)$. Bellow: another example of a permutation contracting indexes of $\mathrm{tr}_A(\rho_A^6)$, this time for $p = (2, 1, 3, 4, 6, 5)$. Bottom: mapping of the contraction of blocks defined in the upper left panel into contraction of indices running over each subspace for the example above; for B indices the mapping is one to one, but in order to recover the contractions of A indices one must compose the permutation with $\pi(i) = (i + 1)\mathrm{mod}(n)$, yielding, for this case, $\pi^{-1} \circ p = (1, 3, 4, 6, 5, 2)$.

sums over free indices a_i and b_i running over orthonormal bases of the subsystems A and B Hilbert spaces, respectively, each free sum resulting in a factor D_A or D_B. While this complicated explanation might not seem helpful at first glance, it points to us that we are interested in averaging over various coupling configurations of the amplitudes' indices. In fact, since the delta function equates indices after coupling, we can translate this problem into a sum over partitions of indices p, which can be visualized in the tensor network representation shown in figure 4.1.

In Figure 4.1 we see that the averages (4.11) have an inherent structure for each subspace's indices represented by the black lines, and we can partition them by coupling

summation indices as represented by the red lines in some examples. We also see that the indices over subspace B are 'aligned' with the tensor amplitudes 'boxes', meaning the partitions done by coupling boxes will translate in a one-to-one fashion to partition of B indices, in which each block of the partition has the same index b_i which is free to sum over the B subspace. We will call each index free to sum as such a *cycle* over B. As can be seen in figure 4.1, the number of cycles in B is the number of blocks k in the partition p, and we define $C(p)$ as the number of cycles (blocks) associated with said partition. Meanwhile, we also see that the number of cycles in subsystem A for a given partition p is given by $C(\pi^{-1} \circ p)$, where $\pi(i) = (i+1)\text{mod}(r)$ corresponds to a shift in indices, as the last sketch exemplifies. This gives us a rule for finding the number of cycles over subspaces A and B of the system. Translating this discussion to mathematical terms we find that:

$$\langle \text{tr}_A(\rho_A^r) \rangle = \frac{1}{D^r} \sum_{p \in S_r} D_A^{C(\pi^{-1} \circ p)} D_B^{C(p)}, \tag{4.13}$$

where S_r stands for the group of permutation of r elements.

We can carry the sum over partitions with the aid of the diagrams in Figure 4.1, but first we can simplify things by looking for leading order contributions. From previous works on this subject [1, 2], it is known that the maximal number of cycles is $C(p) + C(\pi^{-1} \circ p) = r + 1$, which is realized for noncrossing partitions. This means that for a given crossing partition p', the contribution $D_A^{C(p)} D_B^{C(\pi^{-1} \circ p)} / D^r$ is suppressed in powers of $1/D$ relative to the noncrossing partitions' contributions. Thus, one can rewrite the sum above, to leading order in $1/D$, as

$$\langle \text{tr}_A(\rho_A^r) \rangle = \frac{1}{D^r} \sum_{p \in G_r} D_A^{C(\pi^{-1} \circ p)} D_B^{C(p)}, \tag{4.14}$$

where $G_r \in S_r$ stands for the set of noncrossing partitions of r elements. We are now positioned to make use of the combinatorial tools established in the previous section. Since we know that the number of noncrossing partitions of r elements into k cycles is given by the Narayana numbers, and that the maximization of the number of cycles fixes,

for $C(p) = k$:

$$\begin{aligned} C(p) + C(\pi^{-1} \circ p) &= r + 1 \\ k + C(\pi^{-1} \circ p) &= r + 1 \\ C(\pi^{-1} \circ p) &= r - k + 1, \end{aligned}$$

we can write:

$$M_r = \langle \mathrm{tr}_A(\rho_A^r) \rangle = \frac{1}{D^r} \sum_{k=1}^{r} \frac{1}{r} \binom{r}{k} \binom{r}{k-1} D_A^k D_B^{r-k+1}. \tag{4.15}$$

This effectively replaces the sum over partitions by a sum over the number of cycles the partitions can have, weighted by the combinatorial factor given by the Narayana numbers in (3.18).

Before we go further it is important to make a commentary about the above result. Reshaping factors we get:

$$M_r = \sum_{k=1}^{r} \frac{1}{r} \binom{r}{k} \binom{r}{k-1} \frac{D_B}{D_A^r} \left(\frac{D_A}{D_B} \right)^k, \tag{4.16}$$

and we can see clearly that this is an expansion in powers of D_A/D_B, which is convergent for every r only for $D_A \leq D_B$. Therefore the expression above is valid only for the 'first half' of our set of qubits, and we must find another equation for the 'second half', where $D_A > D_B$. Luckily that is a simple task. We can reshape the trace in equation (4.11) to the form

$$\mathrm{tr}_A(\rho_A^r) = \sum_{\{a^i\}} \sum_{\{b^i\}} \bar{\psi}_{a^1 b^r} \psi_{a^1 b^1} \bar{\psi}_{a^2 b^1} \psi_{a^2 b^2} \bar{\psi}_{a^3 b^2} \cdots \psi_{a^r b^r}, \tag{4.17}$$

meaning that we can turn the top-right diagram in Figure 4.1 upside down and the same steps taken above would lead to equation (4.15) with $D_A \leftrightarrow D_B$. Because of that we can proceed by evaluating the EE only for the first half of the qubit set and simply switch D_A with D_B for the second half expression afterwards.

The EE follows then from the replica trick:

$$S(\rho_A) = -\partial_r M_r|_{r=1} = -\partial_r \left\langle \mathrm{tr}_A(\rho_A) \right\rangle |_{r=1}. \tag{4.18}$$

Since we have $\binom{r}{k} = 0$ for $k > r$, we can extend the sum to infinity in (4.15). Substituting

the definition of the binomial:

$$\begin{aligned}\langle Tr(\rho_A^r)\rangle &= \sum_{k=1}^{\infty}\frac{1}{r}\frac{r!}{k!(r-k)!}\frac{r!}{(k-1)!(r+1-k)!}D_A^{k-r}D_B^{1-k}\\ &= \sum_{k=1}^{\infty}\frac{r(r-1)^2(r-2)^2...(r-k+2)^2(r-k+1)}{k!(k-1)!}D_A^{k-r}D_B^{1-k}\\ &= \Bigg[D_A^{1-r}+\frac{r(r-1)}{2}\frac{D_A^{2-r}}{D_B}+\\ &\quad+\sum_{k=3}^{\infty}\frac{r(r-1)^2...(r-k+2)^2(r-k+1)}{k!(k-1)!}D_A^{k-r}D_B^{1-k}\Bigg].\end{aligned} \tag{4.19}$$

As can be seen, if we take the derivative with respect to r followed by the limit $r \to 1$ above, the terms left in the sum will all go to zero, since they all have the factor $(r-1)^2$, and we can safely ignore them in the following calculations. Therefore

$$\begin{aligned}S(\rho_A) &= -\partial_r\left[D_A^{1-r}+\frac{r(r-1)}{2}\frac{D_A^{2-r}}{D_B}\right]\Bigg|_{r=1}\\ &= -\partial_r\left[e^{(1-r)\ln D_A}+\frac{r(r-1)}{2}\frac{e^{(2-r)\ln D_A}}{D_B}\right]\Bigg|_{r=1}\\ &= \left[\ln D_A e^{(1-r)\ln D_A}-\frac{2r-1}{2}\frac{e^{(2-r)\ln D_A}}{D_B}+\frac{r(r-1)}{2}\frac{\ln D_A e^{(2-r)\ln D_A}}{D_B}\right]\Bigg|_{r=1}\\ &= \ln D_A-\frac{D_A}{2D_B},\end{aligned} \tag{4.20}$$

which is Page's result for fully random states.

Equation (4.20) shows that the EE for Haar distributed states is given by a term corresponding to a maximally mixed thermal state ($S_{th} = \ln D_A$) and a correction term. The correction to the fully thermal entropy tells us that some information is stored in the interference between the boundaries of the bipartitioned system. It is however a small correction as it is suppressed by a factor proportional do the system Hilbert spaces' dimension. In Figure 4.2 we see the comparison between the equation above and a simulation with states from the SYK model mentioned and discussed further in chapter 6. We remember that this system is our paradigm for chaos without conservation laws, and we expect their entanglement properties to be properly described by random Haar distributed systems. As we can see the random states have a smaller entropy than a maximally mixed thermal state. The correction, explicit in the second plot, is in great agreement with the

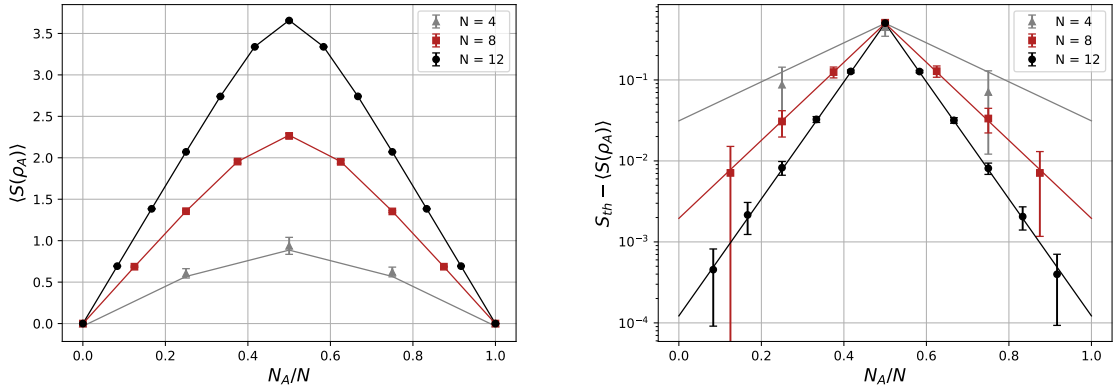

Figure 4.2: In the graphs above we see the Page Eq. (4.20), accompanied by the EE from a simulation of states from a SYK model corresponding to $N = 4, 8, 12$ qubits (see chapter 6 fore more details). Left: plots for the EE predicted analytically and simulated by random states. Right: These are the same plots of the graph in the left, subtracted from the thermal contribution $S_{th} = \ln D_A$ and on logarithmic scale. Also, the points corresponding to $N_A = 0, N$ (yielding $S_A = 0$) where excluded for better presenting the result.

analytical result derived.

4.3 Entanglement Entropy (EE) - Systems with Conservation Laws

In order to evaluate the EE for physical states of chaotic many-body systems, we try to adapt the previous approach to the new conserved quantity requirement. As discussed, this is accomplished by using (4.6) instead of (4.5). In order to carry on, it is helpful to rewrite the summation over the states of the systems as a sum over the quantum numbers

$$\sum_s \to D_S \sum_{Q_S} \Omega_S(Q_S), \qquad s = a, b, \qquad S = A, B. \tag{4.21}$$

Let us now look at how the moments $M_r = \langle \mathrm{tr}_A(\rho_A^r)\rangle$ are written in this setting. Equation (4.12) remains perfectly valid since no assumptions were made up to that point except that we deal with pure states, which is still the case. From there we used combinatorics and the delta function in the amplitudes' variances to find that we are left with a certain number of free index summations over subsystems A and B Hilbert spaces, yielding factors D_A and D_B. The combinatoric arguments are still valid, so we can translate equation (4.15) to this situation by employing the representation above for the free index summations

and making the substitutions $D_A \to D_A\Omega_A(Q_A)$ and $D_B \to D_B\Omega_B(Q-Q_A)$ as well as introducing a summation over Q_A (we already evaluate the summation over Q_B which is trivially done with the delta function $\delta_{Q_A(a)+Q_B(b),Q}$ on (4.6)):

$$, \tag{4.22}$$

where we generalized the spectral distribution defined before to subsystems as $F_S(Q_S) \equiv D_S\Omega_S(Q_S)$, with $S = A, B$. Rearranging the equation, we find:

$$M_r(Q) = \sum_{k=1}^{\infty}\sum_{Q_A}\frac{1}{r}\binom{r}{k}\binom{r}{k-1}\frac{F_B^{r+1}(Q-Q_A)}{F^r(Q)}\left(\frac{F_A(Q_A)}{F_B(Q-Q_A)}\right)^k \tag{4.23}$$

As before, the moments are written as a series, now in powers of $F_A(Q_A)/F_B(Q-Q_A)$. When we previously dealt with this structure for the moments we stated that we must then separate contributions in two parts, as the series will only converge if $F_A/F_B < 1$. While this remains true, additional care must be taken here. Looking at the expression above we see that it is also a sum over the conserved quantity evaluated in subsystem A, Q_A, and since the powers in k in our sum depend on this variable, we must be careful with the summations' limits. Adding these constraints to the moments, we are left to work with the new expression

$$\begin{aligned} M_r(Q) = &\sum_{k=1}^{\infty}\sum_{Q_A} N(r,k)\frac{F_B^{r+1}(Q-Q_A)}{F^r(Q)}\left(\frac{F_A(Q_A)}{F_B(Q-Q_A)}\right)^k \Theta(F_B(Q-Q_A)-F_A(Q_A))+ \\ &+ (A \leftrightarrow B). \end{aligned} \tag{4.24}$$

The Heaviside step-function $\Theta(x)$ introduced here takes care of the cutoff in the Q_A sum, and a second term in which we swap A for B and vice-versa (just as before) is valid for the other region where $F_A(Q_A) > F_B(Q-Q_A)$.

We have seen before that terms with $k \geq 3$ vanish after applying the replica-trick, and that remains true here. Thus:

$$M_r(Q) = \sum_{Q_A} \Bigg[\frac{F_A(Q_A) F_B^r(Q - Q_A)}{F^r(Q)} + \\ + \frac{r(r-1)}{2} \frac{F_A^2(Q_A) F_B^{r-1}(Q - Q_A)}{F^r(Q)} \Bigg] \Theta(F_B(Q - Q_A) - F_A(Q_A)) + (A \leftrightarrow B). \tag{4.25}$$

Taking the replica-trick we arrive at

$$\begin{aligned} S(Q_A) &= -\partial_r M_r(Q)|_{r=1} \\ &= -\sum_{Q_A} \left[\frac{F_A(Q_A) F_B(Q - Q_A)}{F(Q)} \ln \left(\frac{F_B(Q - Q_A)}{F(Q)} \right) + \frac{1}{2} \frac{F_A^2(Q_A)}{F(Q)} \right] \times \\ &\quad \times \Theta(F_B(Q - Q_A) - F_A(Q_A)) + (A \leftrightarrow B). \end{aligned} \tag{4.26}$$

In order to advance from here, we must fix a spectral density for the system. We assume here that, except in the far tails of the spectrum, the spectral density is well approximated by a Gaussian distribution centered around $Q = 0$ as its value of maximal spectral weight

$$, \tag{4.27}$$

with index S referring to subsystems $S = A, B$ or, if omitted, the full system. For a better discussion on the choice of the above distribution we refer to Appendix A.

The equation above allows us to work with generic variables (N_A, Q), although some choices may lead to complicated calculations, we are mainly interested in evaluating the EE at the peak of the spectral density $Q = 0$ where the most universal behaviour is expected. Using the Gaussian spectral density ansatz at $Q = 0$, the step-function in (4.26) reduces to $\Theta(F_B(Q - Q_A) - F_A(Q_A)) \to \Theta(N_B - N_A)$ and, as before, the solution is split into the two halves, with mirrored structure. To see why that is the case we take the derivative of $F_A(Q_A)$ with respect to N_A:

$$\partial_{N_A} F_A(Q_A, N_A) = \partial_{N_A}\left[\frac{2^{N_A}}{\sqrt{2\pi\gamma^2 N_A}} e^{-\frac{Q_A^2}{2\gamma^2 N_A}}\right] = \frac{2^{N_A}}{\sqrt{2\pi\gamma^2 N_A}} e^{-\frac{Q_A^2}{2\gamma^2 N_A}}\left[\ln 2 - \frac{1}{2N_A} + \frac{Q_A^2}{2\gamma^2 N_A^2}\right]. \tag{4.28}$$

The above expression is positive for all positive integer values for N_A, meaning $F_A(Q_A)$ is strictly increasing throughout the range we are interested. On the other hand, $F_B(-Q_A)$ (remember we set $Q = 0$) is strictly decreasing in the same interval as it is a function of $N_B = N - N_A$. Since equality occurs when $N_A = N_B = N/2$ at $Q = 0$ and for $N_A = 1$ we clearly have $F_B > F_A$. It follows that $\Theta(F_B(Q - Q_A) - F_A(Q_A)) \to \Theta(N_B - N_A)$.

We now move on to evaluate the sums over Q_A in (4.26). In order to do so, we will look to approximate the sums as integrals. Introducing $q_S = Q_S/N$ such that $dq_S \sim 1/N$, we can make the connection we seek. Solving each term in (4.26) at a time we find:

$$\begin{aligned}
-\sum_{Q_A} \frac{F_A(Q_A)F_B(-Q_A)}{F(0)} \ln\left[\frac{F_B(-Q_A)}{F(0)}\right] &= -\sum_{Q_A} \sqrt{\frac{N}{2\pi\gamma^2 N_A N_B}} e^{-\frac{Q_A^2}{2\gamma^2 N_A}} e^{-\frac{Q_A^2}{2\gamma^2 N_B}} \times \\
&\qquad \times \ln\left[\frac{D_B}{D}\sqrt{\frac{N}{N_B}} e^{-\frac{Q_A^2}{2\gamma^2 N_B}}\right] \\
&= -\int dq_A \sqrt{\frac{N^3}{2\pi\gamma^2 N_A N_B}} e^{-\frac{N^2 q_A^2}{2\gamma^2 N_A}} e^{-\frac{N^2 q_A^2}{2\gamma^2 N_B}} \left(\ln\left[\frac{1}{D_A}\sqrt{\frac{N}{N_B}}\right] - \frac{N^2 Q_A^2}{2\gamma^2 N_B}\right) \\
&= \ln D_A - \frac{1}{2}\ln\frac{N}{N_B} + \frac{N_A}{2N},
\end{aligned} \tag{4.29}$$

and

$$\begin{aligned}
-\frac{1}{2}\sum_{Q_A} \frac{F_A^2(Q_A)}{F(0)} &= -\frac{1}{2}\sum_{Q_A} \frac{1}{N_A}\sqrt{\frac{N}{2\pi\gamma^2}} \frac{D_A^2}{D} e^{-\frac{2Q_A^2}{2\gamma^2 N_A}} = -\frac{1}{2N_A}\frac{D_A^2}{D}\int dq_A \sqrt{\frac{N^3}{2\pi\gamma^2}} e^{-\frac{2N^2 q_A^2}{2\gamma^2 N_A}} \\
&= -\sqrt{\frac{N}{2N_A}}\frac{D_A}{2D_B}.
\end{aligned} \tag{4.30}$$

Gathering terms we find

$$S(\rho_A) = \ln D_A - \frac{1}{2}\ln\frac{N}{N_B} + \frac{N_A}{2N} - \sqrt{\frac{N}{2N_A}}\frac{D_A}{2D_B}. \tag{4.31}$$

We remember that for $N_A > N_B$ one must take $N_A \leftrightarrow N_B$ as we did for Page states. This

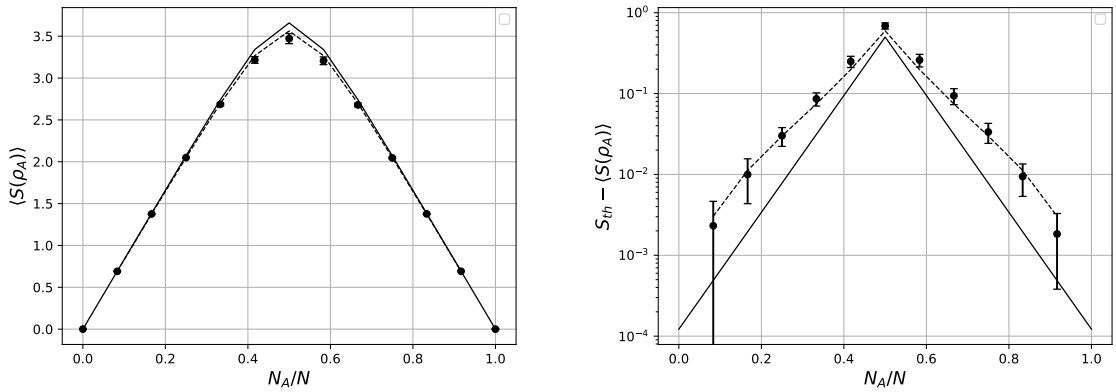

Figure 4.3: In the plots above we see two presentations of the same result, in analogy to Figure 4.2. The solid line shows the analytical prediction for Page states' EE given by (4.20) and the dotted line shows the equation for states with conservation laws given by (4.31). The data points are for a spin-1/2 of length $N = 12$ which conserves total energy, with the EE averaged over 10 energy eigenstates with energy close to the maximum spectral weight. Here we choose to present only results for $N = 12$ for better readability. We see great agreement between simulation and (4.31).

is the main result of this section and it reproduces the result of previous work Ref. [3]. In Figure 4.3 we see the analytical result above, together with the prediction for Page states given by (4.20) and data points from the simulation of a spin-1/2 chain which is expected to be described by this section's formalism as it has local energy conservation. For a more in depth presentation and discussion of this model we refer to Chapter 6. As we can see, the corrections to Page's result developed above are in excellent agreement with the simulation, validating the result obtained.

As a minor result we now look at systems with a non-zero finite charge $Q \neq 0$. We choose to focus solely on the point $N_A = N_B = N/2$, which greatly simplifies the step-function cutoff in (4.26). Explicitly writing the condition for the step-function $\Theta(F_B(Q - Q_A) - F_A(Q_A))$ we find:

$$
\begin{aligned}
F_B(Q-Q_A) &> F_A(Q_A) \\
D_B\Omega_B(Q-Q_A) &> D_A\Omega_A(Q_A) \\
2^{N_B}\sqrt{\frac{1}{2\pi\gamma^2 N_B}}e^{-\frac{(Q-Q_A)^2}{2\gamma^2 N_B}} &> 2^{N_A}\sqrt{\frac{1}{2\pi\gamma^2 N_A}}e^{-\frac{Q_A^2}{2\gamma^2 N_A}} \\
\exp\left[\frac{Q_A^2}{2\gamma^2 N_A}-\frac{(Q-Q_A)^2}{2\gamma^2 N_B}\right] &> 2^{N_A-N_B}\sqrt{\frac{N_B}{N_A}} \\
Q_A^2\left(\frac{N_B-N_A}{2\gamma^2 N_A N_B}\right)+Q_A\frac{Q}{\gamma^2 N_B}-\frac{Q^2}{2\gamma^2 N_B} &> \ln\left[2^{N_A-N_B}\sqrt{\frac{N_B}{N_A}}\right].
\end{aligned}
\tag{4.32}
$$

Setting $N_A = N_B = N/2$ we get $Q_A > Q/2$, which must be respected when evaluating the sum over Q_A in equation (4.26). Turning our attention to said equation we see that we can rewrite this using $\sum_{Q_A}(...)\Theta(F_B - F_A) = \sum_{Q_A}(...) - \sum_{Q_A}(...)\Theta(F_A - F_B)$. We can thus identify two contributions in (4.26), a leading one:

$$
S_L = -\sum_{Q_A}\left[\frac{F_A(Q_A)F_B(Q-Q_A)}{F(Q)}\ln\left(\frac{F_B(Q-Q_A)}{F(Q)}\right)+\frac{1}{2}\frac{F_A^2(Q_A)}{F(Q)}\right],
\tag{4.33}
$$

and a correction:

$$
\begin{aligned}
\delta S =& \sum_{Q_A}\left[\frac{F_A(Q_A)F_B(Q-Q_A)}{F(Q)}\ln\left(\frac{F_B(Q-Q_A)}{F(Q)}\right)+\frac{1}{2}\frac{F_A^2(Q_A)}{F(Q)}+\right. \\
&\left.-\frac{F_B(Q-Q_A)F_A(Q_A)}{F(Q)}\ln\left(\frac{F_A(Q_A)}{F(Q)}\right)-\frac{1}{2}\frac{F_B^2(Q-Q_A)}{F(Q)}\right]\Theta(F_A(Q_A)-F_B(Q-Q_A)) \\
=& \sum_{Q_A<Q/2}\left[\frac{F_A(Q_A)F_B(Q-Q_A)}{F(Q)}\ln\left(\frac{F_B(Q-Q_A)}{F_A(Q_A)}\right)+\frac{1}{2}\frac{F_A^2(Q_A)-F_B^2(Q-Q_A)}{F(Q)}\right].
\end{aligned}
\tag{4.34}
$$

Let us begin evaluating the leading contribution. Using the Gaussian density of states in (4.27) (remember we are at $N_A = N_B = N/2$)

$$
\begin{aligned}
S_L =& -\sum_{Q_A}\left[\frac{F_A(Q_A)F_B(Q-Q_A)}{F(Q)}\ln\left(\frac{F_B(Q-Q_A)}{F(Q)}\right)+\frac{1}{2}\frac{F_A^2(Q_A)}{F(Q)}\right]\\
=& -\sum_{Q_A}\left[\frac{D_A\sqrt{\frac{1}{2\pi\gamma^2N_A}}e^{-\frac{Q_A^2}{2\gamma^2N_A}}D_B\sqrt{\frac{1}{2\pi\gamma^2N_B}}e^{-\frac{(Q-Q_A)^2}{2\gamma^2N_B}}}{D\sqrt{\frac{1}{2\pi\gamma^2N}}e^{-\frac{Q^2}{2\gamma^2N}}}\ln\left(\frac{D_B\sqrt{\frac{1}{2\pi\gamma^2N_B}}e^{-\frac{(Q-Q_A)^2}{2\gamma^2N_B}}}{D\sqrt{\frac{1}{2\pi\gamma^2N}}e^{-\frac{Q^2}{2\gamma^2N}}}\right)+\right.\\
&\left.+\frac{1}{2}\frac{D_A^2\frac{1}{2\pi\gamma^2N_A}e^{-\frac{2Q_A^2}{2\gamma^2N_A}}}{D\sqrt{\frac{1}{2\pi\gamma^2N}}e^{-\frac{Q^2}{2\gamma^2N}}}\right]\\
=& -\sum_{Q_A}\sqrt{\frac{2}{\pi\gamma^2N}}\left[\exp\left(\frac{-(2Q_A-Q)^2}{2\gamma^2N}\right)\ln\left(2^{\frac{1}{2}-\frac{N}{2}}\exp\left(\frac{Q^2-2(Q_A-Q)^2}{2\gamma^2N}\right)\right)+\right.\\
&\left.+\frac{1}{2}\exp\left(\frac{Q^2-4Q_A^2}{2\gamma^2N}\right)\right].
\end{aligned}
\tag{4.35}
$$

Now we substitute $q_S = Q_A/N$, and introduce the 'infinitesimal' $dq_A \sim 1/N$ that will allow us to translate the sum into an integral

$$
\begin{aligned}
S_L =& -\sum_{q_A}\sqrt{\frac{2}{\pi\gamma^2N}}\left[\exp\left(\frac{-N(2q_A-q)^2}{2\gamma^2}\right)\ln\left(2^{\frac{1}{2}-\frac{N}{2}}\exp\left(\frac{Nq^2-N2(q_A-q)^2}{2\gamma^2}\right)\right)+\right.\\
&\left.+\frac{1}{2}\exp\left(\frac{N(q^2-4q_A^2)}{2\gamma^2}\right)\right]\\
=& -\int dq_A\sqrt{\frac{2N}{\pi\gamma^2}}\left[\exp\left(\frac{-N(2q_A-q)^2}{2\gamma^2}\right)\ln\left(2^{\frac{1}{2}-\frac{N}{2}}\exp\left(\frac{Nq^2-N2(q_A-q)^2}{2\gamma^2}\right)\right)+\right.\\
&\left.+\frac{1}{2}\exp\left(\frac{N(q^2-4q_A^2)}{2\gamma^2}\right)\right].
\end{aligned}
\tag{4.36}
$$

Solving one integral at a time

$$
\begin{aligned}
&\int dq_A \exp\left(\frac{-N(2q_A-q)^2}{2\gamma^2}\right)\ln\left(2^{\frac{1}{2}-\frac{N}{2}}\exp\left(\frac{Nq^2-N2(q_A-q)^2}{2\gamma^2}\right)\right)= \\
&\quad=\int dq_A \exp\left(\frac{-N(2q_A-q)^2}{2\gamma^2}\right)\left[\frac{1-N}{2}\ln 2+\frac{Nq^2-N2(q_A-q)^2}{2\gamma^2}\right] \\
&\quad=\left(\frac{1-N}{2}\ln 2+\frac{Nq^2}{2\gamma^2}\right)\int dq_A \exp\left(\frac{-N(2q_A-q)^2}{2\gamma^2}\right)+ \\
&\qquad+\int dq_A \exp\left(\frac{-N(2q_A-q)^2}{2\gamma^2}\right)\frac{-N(q_A-q)^2}{\gamma^2}\Bigg] \\
&\quad=\left(\frac{1-N}{2}\ln 2+\frac{Nq^2}{2\gamma^2}\right)\sqrt{\frac{\pi\gamma^2}{2N}}-\frac{1}{4}\sqrt{\frac{\pi N}{2\gamma^2}}q^2-\frac{1}{4}\sqrt{\frac{\pi\gamma^2}{2N}},
\end{aligned}
\tag{4.37}
$$

$$
\int dq_A \frac{1}{2}\exp\left(\frac{N(q^2-4q_A^2)}{2\gamma^2}\right)\Bigg]=\frac{1}{2}\sqrt{\frac{\pi\gamma^2}{2N}}e^{\frac{Nq^2}{2\gamma^2}}. \tag{4.38}
$$

Gathering results we get

$$
S_L=\frac{N-1}{2}\ln 2-\frac{Nq^2}{4\gamma^2}+\frac{1}{4}-\frac{1}{2}e^{\frac{Nq^2}{2\gamma^2}} \tag{4.39}
$$

The correction yields

$$
\begin{aligned}
\delta S=&\sum_{Q_A<Q/2}\left[\frac{F_A(Q_A)F_B(Q-Q_A)}{F(Q)}\ln\left(\frac{F_B(Q-Q_A)}{F_A(Q_A)}\right)+\frac{1}{2}\frac{F_A^2(Q_A)-F_B^2(Q-Q_A)}{F(Q)}\right] \\
=&\sum_{Q_A<\frac{Q}{2}}\sqrt{\frac{2}{\pi\gamma^2 N}}\Bigg[\exp\left(\frac{-(2Q_A-Q)^2}{2\gamma^2 N}\right)\frac{2QQ_A-Q^2}{\gamma^2 N}+ \\
&+\frac{1}{2}\exp\left(\frac{Q^2-4Q_A^2}{2\gamma^2 N}\right)-\frac{1}{2}\exp\left(\frac{Q^2-4(Q-Q_A)^2}{2\gamma^2 N}\right)\Bigg] \\
=&\int_{q_A<\frac{q}{2}}dq_A\sqrt{\frac{2N}{\pi\gamma^2}}\Bigg[\exp\left(\frac{-N(2q_A-q)^2}{2\gamma^2}\right)\frac{2Nqq_A-Nq^2}{\gamma^2}+ \\
&+\frac{1}{2}\exp\left(\frac{Nq^2-4Nq_A^2}{2\gamma^2}\right)-\frac{1}{2}\exp\left(\frac{Nq^2-4N(q-q_A)^2}{2\gamma^2}\right)\Bigg] \\
=&\frac{1}{2}e^{\frac{Nq^2}{2\gamma^2}}\operatorname{erf}\left(\sqrt{\frac{N}{2\gamma^2}}q\right)-\sqrt{\frac{N}{2\pi\gamma^2}}q.
\end{aligned}
\tag{4.40}
$$

Gathering all terms we get the EE at $N_A = N_B = N/2$

$$\begin{aligned} S(\rho_A; N_A = N_B) =& \frac{N-1}{2}\ln 2 - \frac{Nq^2}{4\gamma^2} + \frac{1}{4} - \frac{1}{2}e^{\frac{Nq^2}{2\gamma^2}} + \frac{1}{2}e^{\frac{Nq^2}{2\gamma^2}}\,\mathrm{erf}\left(\sqrt{\frac{N}{2\gamma^2}}q\right) - \sqrt{\frac{N}{2\pi\gamma^2}}q \\ =& \frac{N-1}{2}\ln 2 - \frac{Q^2}{4\gamma^2 N} + \frac{1}{4} - \frac{1}{2}e^{\frac{Q^2}{2\gamma^2 N}}\,\mathrm{Erfc}\left(\frac{Q}{\sqrt{2\gamma^2 N}}\right) - \frac{Q}{\sqrt{2\pi\gamma^2 N}}. \end{aligned} \tag{4.41}$$

Thus, as we move further from $Q = 0$ we expect that the EE at half-partition is lowered. We must point however that this behaviour should describe well the vicinity of $Q = 0$ only, we make no predictions concerning the far tails of the distribution.

4.4 Relative Entropy (RE) - Page states

We now wrap the chapter by turning to the relative entropy. The procedure here follows closely the one we employed in the section on the EE for Page states. The replica trick we wish to apply is [27]:

$$S(\rho_A||\sigma_A) \equiv -\,\mathrm{tr}_A(\rho_A \log \sigma_A) - S(\rho_A) = -\partial_r M'_r|_{r=1} - S(\rho_A), \tag{4.42}$$

with the moments $M'_r \equiv \left\langle \mathrm{tr}_A(\rho_A \sigma_A^{r-1}) \right\rangle$. Thankfully, we can make use of the discussion from the EE section on Page states to quickly evaluate these moments. We can expand both ρ_A and σ_A in the same $|a, b\rangle$ basis and find that:

$$\mathrm{tr}_A(\rho_A \sigma_A^{r-1}) = \sum_{\{a^i\}} \sum_{\{b^i\}} \psi^{\rho}_{a^1 b^1} \bar{\psi}^{\rho}_{a^2 b^1} \psi^{\sigma}_{a^2 b^2} \bar{\psi}^{\sigma}_{a^3 b^2} \cdots \psi^{\sigma}_{a^r b^r} \bar{\psi}^{\sigma}_{a^1 b^r}. \tag{4.43}$$

But the variables associated with ρ and σ are uncorrelated and cannot be paired to avoid the random phase cancellation. Therefore the first pair of ψ's must be coupled together, and the last $r-1$ must couple among themselves. If we look at Figure 4.1 and impose that the first square of indices must couple separately, we see that it contributes with a cycle in B and none in A, and that the last $r-1$ couple according to the Narayana

numbers like the case for the EE. We then have

$$\begin{aligned} M'_r = \left\langle \mathrm{tr}_A(\rho_A \sigma_A^{r-1}) \right\rangle &= \frac{1}{(D_A D_B)^r} D_B \sum_{k=1}^{r-1} N(r-1,k) D_A^k D_B^{r-k} \\ &= \frac{1}{(D_A D_B)^r} \sum_{k=1}^{r-1} \frac{1}{r-1} \binom{r-1}{k} \binom{r-1}{k-1} D_A^k D_B^{r-k+1} \\ &= \frac{1}{(D_A D_B)^r} \sum_{k=1}^{r-1} \frac{1}{r-k} \binom{r-1}{k} \binom{r-2}{k-1} D_A^k D_B^{r-k+1}. \end{aligned} \tag{4.44}$$

From here, we proceed just as in the case for the EE

$$\begin{aligned} \langle Tr(\rho_A \sigma_A^{r-1}) \rangle =& \frac{1}{(D_A D_B)^r} \sum_{k=1}^{n-1} \frac{1}{r-k} \binom{r-1}{k} \binom{r-2}{k-1} D_A^k D_B^{r+1-k} \\ =& \sum_{k=1}^{\infty} \frac{1}{r-k} \frac{(r-1)!}{k!(r-k-1)!} \frac{(r-2)!}{(k-1)!(r-k-1)!} D_A^{k-r} D_B^{1-k} \\ =& \sum_{k=1}^{\infty} \frac{(r-1)(r-2)...(r-k)(r-2)(r-3)...(r-k+1)}{k!(k-1)!} D_A^{k-r} D_B^{1-k} \\ =& \sum_{k=1}^{\infty} \frac{(r-1)(r-2)^2(r-3)^2...(r-k+1)^2(r-k)}{k!(k-1)!} D_A^{k-r} D_B^{1-k} \\ =& D_A^{1-r} + \frac{(r-1)(r-2)}{2} \frac{D_A^{2-r}}{D_B} \\ &+ \sum_{k=3}^{\infty} \frac{(r-1)(r-2)^2...(r-k+1)^2(r-k)}{k!(k-1)!} D_A^{k-r} D_B^{1-k}. \end{aligned} \tag{4.45}$$

Then

$$\begin{aligned} \partial_r \langle Tr(\rho_A \sigma_A^{r-1}) \rangle =& \partial_r \left[D_A^{1-r} + \frac{(r-1)(r-2)}{2} \frac{D_A^{2-r}}{D_B} + \right. \\ &\left. + \sum_{k=3}^{\infty} \frac{(r-1)(r-2)^2...(r-k+1)^2(r-k)}{k!(k-1)!} D_A^{k-r} D_B^{1-k} \right] \\ =& \partial_r e^{(1-r)\ln D_A} + \\ &+ \partial_r (r-1) \cdot \left[\frac{r-2}{2} \frac{D_A^{2-r}}{D_B} \right] + (r-1) \cdot \partial_r \left[\frac{r-2}{2} \frac{D_A^{2-r}}{D_B} \right] + \\ &+ \sum_{k=3}^{\infty} \partial_r (r-1) \cdot \frac{(r-2)^2...(r-k+1)^2(r-k)}{k!(k-1)!} D_A^{k-r} D_B^{1-k} \\ &+ \sum_{k=3}^{\infty} (r-1) \partial_r \left[\frac{(r-2)^2...(r-k+1)^2(r-k)}{k!(k-1)!} D_A^{k-r} D_B^{1-k} \right]. \end{aligned} \tag{4.46}$$

Now, since we wish to take the limit $r = 1$, the terms that depend on $(r-1)$ vanish,

and can be ignored in the following calculations,

$$\begin{aligned}\partial_r\langle Tr(\rho_A\sigma_A^{r-1})\rangle|_{r=1} =& \Bigg[- e^{(1-r)\ln D_A}\ln D_A + \frac{r-2}{2}\frac{D_A^{2-r}}{D_B} + \\ &+ \sum_{k=3}^{\infty}\frac{(r-2)^2...(r-k+1)^2(r-k)}{k!(k-1)!}D_A^{k-r}D_B^{1-k}\Bigg]\Bigg|_{r=1} \\ =& -\ln D_A - \frac{D_A}{2D_B} + \sum_{k=3}^{\infty}\frac{(-1)^2...(2-k)^2(1-k)}{k!(k-1)!}\left(\frac{D_A}{D_B}\right)^{k-1}.\end{aligned} \tag{4.47}$$

To proceed we rewrite the summation as

$$\begin{aligned}\sum_{k=3}^{\infty}\frac{(-1)^2...(2-k)^2(1-k)}{k!(k-1)!}\left(\frac{D_A}{D_B}\right)^{k-1} =& \sum_{k=3}^{\infty}\frac{(1)^2...(k-2)^2(k-1)^2}{k!(k-1)!(1-k)}\left(\frac{D_A}{D_B}\right)^{k-1} \\ =& \sum_{k=3}^{\infty}\frac{((k-1)!)^2}{k!(k-1)!(1-k)}\left(\frac{D_A}{D_B}\right)^{k-1} \\ =& \sum_{k=3}^{\infty}\frac{1}{k(1-k)}\left(\frac{D_A}{D_B}\right)^{k-1}.\end{aligned} \tag{4.48}$$

Substituting this in our RE, written in terms of replica tricks as

$$S(\rho_A||\sigma_A) = \partial_r\langle Tr(\rho_A^r)\rangle|_{r=1} - \partial_r\langle Tr(\rho_A\sigma_A^{r-1})\rangle|_{r=1}, \tag{4.49}$$

together with Page's result for the first term from the previous section

$$\begin{aligned}S(\rho_A||\sigma_A) =& \frac{D_A}{D_B} + \sum_{k=3}^{\infty}\frac{1}{k(k-1)}\left(\frac{D_A}{D_B}\right)^{k-1} = \frac{D_A}{D_B} + \sum_{k=3}^{\infty}\left[\frac{1}{k-1} - \frac{1}{k}\right]\left(\frac{D_A}{D_B}\right)^{k-1} \\ =& \frac{D_A}{D_B} + \sum_{k=3}^{\infty}\frac{1}{k-1}\left(\frac{D_A}{D_B}\right)^{k-1} - \sum_{k=3}^{\infty}\frac{1}{k}\left(\frac{D_A}{D_B}\right)^{k-1} \\ =& \frac{D_A}{D_B} + \left[\sum_{k=1}^{\infty}\frac{1}{k}\left(\frac{D_A}{D_B}\right)^{k} - \frac{D_A}{D_B}\right] + \\ &- \frac{D_B}{D_A}\left[\sum_{k=1}^{\infty}\frac{1}{k}\left(\frac{D_A}{D_B}\right)^{k} - \frac{D_A}{D_B} - \frac{1}{2}\left(\frac{D_A}{D_B}\right)^{2}\right].\end{aligned} \tag{4.50}$$

Using now

$$\ln(1-x) = -\sum_{n=1}^{\infty}\frac{x^n}{n}, \tag{4.51}$$

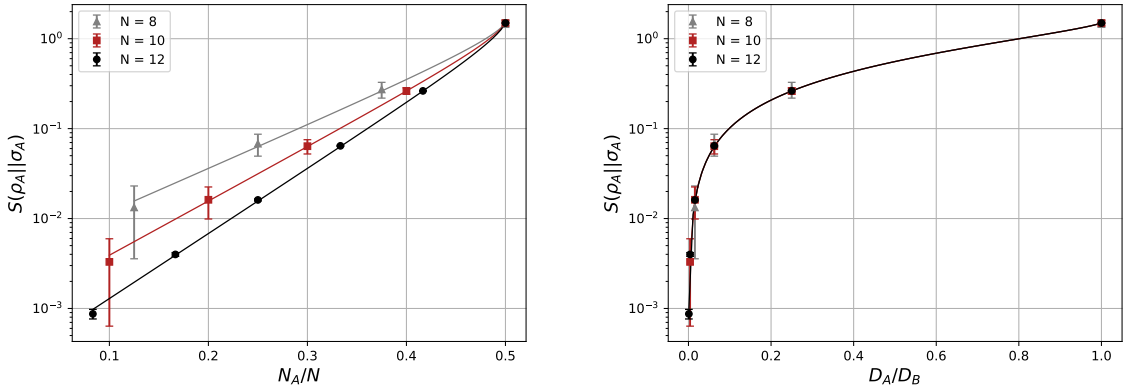

Figure 4.4: Figures above show results for the RE from a simulation of eigenstates of the SYK model corresponding to $N = 8, 10, 12$ qubit systems, accompanied by the analytical prediction, given by equation (4.52). Both figures show the same data on linear (left) and logarithmic (right) scales, respectively.

we have

$$\begin{aligned} S(\rho_A||\sigma_A) =& \frac{D_A}{D_B} + \left[-\ln\left(1 - \frac{D_A}{D_B}\right) - \frac{D_A}{D_B}\right] + \\ & - \frac{D_B}{D_A}\left[-\ln\left(1 - \frac{D_A}{D_B}\right) - \frac{D_A}{D_B} - \frac{1}{2}\left(\frac{D_A}{D_B}\right)^2\right] \\ =& 1 + \left(\frac{D_B}{D_A} - 1\right)\ln\left(1 - \frac{D_A}{D_B}\right) + \frac{D_A}{2D_B}. \end{aligned} \tag{4.52}$$

This reproduces previous results in Ref. [8] and recovers two notable limits pointed, namely:

$$\begin{aligned} S(\rho_A||\sigma_A) &\to 0 \quad \text{as} \quad \frac{D_A}{D_B} \to 0, \\ S(\rho_A||\sigma_A) &\to \frac{3}{2} \quad \text{as} \quad \frac{D_A}{D_B} \to 1. \end{aligned} \tag{4.53}$$

In Figure 4.4 we can see the results of the simulations for SYK states as well as the analytical prediction above for these states. We note that the figures are found only up to $N_A = N/2$, as for $N_A > N$ the RE is defined to be infinite according to the properties presented on chapter 2.

We are now positioned to better grasp the conceptual difficulty of conciliating the RE with the approach for eigenstates of systems which conserve a local charge. The employment of the density of states in Eq. (4.21) when evaluating the EE for such states

leads us to Eq. (4.24), which is series in powers of the ratio of spectral distributions for each subsystem. The convergence of the sum hinges upon the requirement fixed with the Heaviside step function, namely $F_A(Q_A) < F_B(Q - Q_A)$ (or the opposite depending on the term). This requirement is not restricted to subsystem A or B, rather how the charge is distributed, and thus takes input from the whole system. This goes against the fact that the RE is infinite if we cross the subsystems' boundaries. Therefore, we did not explore the RE for eigenstates of systems with conservation laws.

4.5 Summary

We have thus managed to reproduce in this section some interesting results on the literature regarding entanglement properties of random states. Amongst the main predictions in the chapter are fully analytical descriptions for the entanglement entropy for both Page states Eq. (4.20), in agreement with Page's original result [7], and for eigenstates of systems which locally conserve some charge Eq. (4.31) reproducing Ref. [3]. Together with these we also developed an analytical description for the relative entropy of Page states Eq. (4.52) which is in accordance with previous work Ref. [8]. Unfortunately, the extension of the relative entropy for charge eigenstates was not accomplished here.

Finally, we have in this chapter introduced and and gained familiarity with (most of) the machinery needed to tackle the trace distance in the next chapter, the main chapter in this dissertation.

Chapter 5

Trace Distance

We next present the main and novel results of this dissertation: analytical predictions for the trace distance of ergodic states both with and without conservation laws. While the TD for Page states has been studied before [9], no close analytical results have been obtained to our knowledge. We here provide fully analytical results from solving the combinatorial problem at the hearth of the replica-trick exactly. Moreover we discuss ergodic states with local conservations laws.

5.1 Trace Distance (TD) - Page states

In this section we develop the main result of this work, that is, an analytical formula for the trace distance of random states. We follow the same lines as with the chapter.

For the replica trick for the trace distance we need to evaluate $M_r'' \equiv \mathrm{tr}_A([\rho_A - \sigma_A]^r)$, and the replica-trick established in Ref. [28] tells us that

$$\langle D_1(\rho_A, \sigma_A)\rangle = \frac{1}{2}\lim_{r_e\to 1} M_{r_e} = \frac{1}{2}\lim_{r_e\to 1}\langle \mathrm{tr}_A([\rho_A - \sigma_A]^{r_e})\rangle\,, \tag{5.1}$$

where r_e stands for even moments. We can write the above in a more useful form by expanding both density matrices in the $|a, b\rangle$ basis

$$\begin{aligned}\mathrm{tr}_A([\rho_A - \sigma_A]^r) &= \sum_{a''}\langle a''|\left[\sum_{a,a'}\sum_{b}\left(\psi^{\rho}_{ab}\bar{\psi}^{\rho}_{a'b} - \psi^{\sigma}_{ab}\bar{\psi}^{\sigma}_{a'b}\right)|a'\rangle\langle a|\right]^r|a''\rangle \\ &= \sum_{\{\alpha^i=\rho,\sigma\}}\sum_{\{a^i\}}\sum_{\{b^i\}}\mathrm{sgn}(\sigma)\psi^{\alpha^1}_{a^1b^1}\bar{\psi}^{\alpha^1}_{a^2b^1}\psi^{\alpha^2}_{a^2b^2}\bar{\psi}^{\alpha^2}_{a^3b^2}\cdots\psi^{\alpha^r}_{a^rb^r}\bar{\psi}^{\alpha^r}_{a^1b^r},\end{aligned} \tag{5.2}$$

where $\mathrm{sgn}(\sigma) = \pm 1$ if an even/odd number of σ_A density matrices are involved in the product. For each matrix the amplitudes follow Page's, i.e.

$$\left\langle \psi_n^\rho \bar{\psi}_m^\rho \right\rangle = \frac{\delta_{nm}}{D}, \qquad \left\langle \psi_n^\sigma \bar{\psi}_m^\sigma \right\rangle = \frac{\delta_{nm}}{D}, \tag{5.3}$$

with uncorrelated moments involving amplitudes from different matrices

$$\left\langle \psi_n^\rho \bar{\psi}_m^\sigma \right\rangle = \left\langle \psi_n^\sigma \bar{\psi}_m^\rho \right\rangle = 0. \tag{5.4}$$

Again, we resort to diagrams for the bookkeeping of summation. More specifically, we extend the code in diagram 4.1 to allow for another index α which tracks the density matrix to which a given amplitude is associated. The result is Figure 5.1. Again we look to couple variables in order to avoid random phase cancellation. We now have to account for the third index α in equation (5.2), which is fixed within each block of the partition. Now, blocks with an odd number of elements can be either all from the ρ density matrix or from the σ density matrix, and for each of these cases the absolute value of the average are the same but with opposite signs since for an odd number of σ elements the overall sign of the average is negative. Because of this, these blocks cancel in every partition containing them, and all partitions with odd total number of elements effectively. For finite contributions, we thus must restrict ourselves to partitions in blocks with even elements in which the sign is the same whether $\alpha = \rho$ or $\alpha = \sigma$. Following our discussion of the EE we see that the number of cycles in subspace B for a partition in k blocks is k and in subspace A it is $r - k + 1$. In section 3 we evaluated the number $N_e(r, k)$ of partitions allowed with k cycles and blocks containing an even number of elements. Using this results we find

$$\begin{aligned} M_r'' = \langle \mathrm{tr}_A([\rho_A - \sigma_A]^r) \rangle =& \frac{1}{D^r} \sum_{k=1}^{r/2} 2^k N_e(r,k) D_A^{r-k+1} D_B^k \\ =& \frac{1}{(D_A D_B)^r} \sum_{k=1}^{r/2} \frac{2^{k+1}}{r} \binom{r/2}{k} \binom{r}{k-1} D_A^{r-k+1} D_B^k, \end{aligned} \tag{5.5}$$

and we note that there is two possible values for α in each block, enhancing the number of partitions by a factor of 2^k. We then seek for an analytical continuation of the above expression to all values of r (not even values only), in order to evaluate the TD according

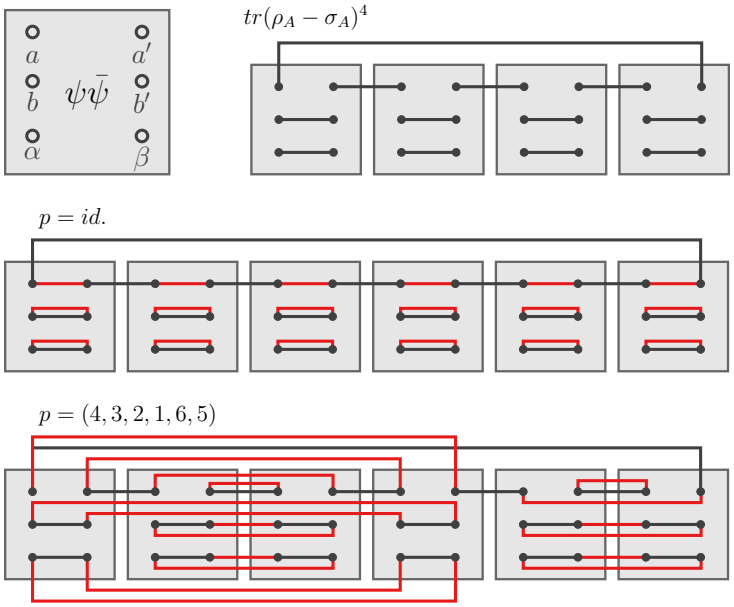

Figure 5.1: Tensor network representation of averages Eq. (5.2). Top left: Following 4.1, tensor network representation $\psi^{\alpha}_{ab}\bar{\psi}^{\alpha}_{a'b}$, now with the new index $\alpha = \rho, \sigma$. Each dot represents an index to be contracted, and contractions must be between right- and left-side indices. Top right: Structure of $\mathrm{tr}(\rho_A - \sigma_A)^4$, with black lines representing index contractions resulting from matrix multiplication in subspace A (top line), traces in subspace B (middle line), and state indices $\alpha = \rho, \sigma$ (bottom line). Notice that the index structure of states follows that of subspace B. Middle: Resulting index structure for $n = 6$ and identity permutation $p = id$. This establishes six B-cycles each consisting of one element, i.e. in the notation of main text $\Lambda_6 = (1^6, 2^0, 3^0, 4^0, 5^0, 6^0)$. Bottom: Another example of a non-crossing permutation for $n = 6$, $p = (4, 3, 2, 1, 6, 5)$. This permutation establishes three B-cycles each consisting of two elements, $\Lambda_6 = (1^0, 2^3, 3^0, 4^0, 5^0, 6^0)$. In the middle diagram, contributions from states ρ (positive sign) and σ (negative sign) sum to zero in each of the one-element cycles. In the bottom diagram contributions from ρ and σ both come with positive sign and sum to two, i.e. contributions from the three cycles add up to $2^3 = 8$.

to our replica-trick.

Expanding the summation and extending it to infinity (the binomials are all zero for $k > r_e/2$)

$$\begin{aligned}
\langle D_1^{(2)}(\rho_A, \sigma_A)\rangle &= \frac{1}{2}\lim_{r\to 1}\sum_{k=1}^{\infty}\frac{2^{k+1}}{r}\binom{r/2}{k}\binom{r}{k-1}D_A^{1-k}D_B^{k-r} \\
&= \lim_{r\to 1}\sum_{k=0}^{\infty}\frac{2^{k+1}}{r}\binom{r/2}{k+1}\binom{r}{k}D_A^{-k}D_B^{k+1-r} \\
&= \lim_{r\to 1} D_B^{1-r}\sum_{k=0}^{\infty}\frac{2}{r}\frac{(r/2)!}{(k+1)!(r/2-k-1)!}\frac{r!}{k!(r-k)!}\left(\frac{2D_B}{D_A}\right)^k \\
&= \lim_{r\to 1} D_B^{1-r}\sum_{k=0}^{\infty}\frac{(r/2-1)!}{(r/2-1-k)!}\frac{r!}{(r-k)!}\frac{(2-1)!}{(2-1+k)!}\frac{(2D_B/D_A)^k}{k!}.
\end{aligned} \tag{5.6}$$

Now, this is an infinite series in powers of $2D_B/D_A$, which only converges if $2D_B \leq D_A$. Because of this we introduced the superscript '(2)' that indicates that this result only holds for $2D_B \leq D_A$.

Using the definitions of the falling factorial and rising factorial (Pochhammer symbol)

$$\begin{aligned}(x)_n &= x(x-1)(x-2)\cdots(x-n+1) = \frac{x!}{(x-n)!} \\ x^{(n)} &= x(x+1)(x+2)\cdots(x+n-1) = \frac{(x+n-1)!}{(x-1)},\end{aligned} \tag{5.7}$$

we can write

$$\langle D_1^{(2)}(\rho_A, \sigma_A)\rangle = \lim_{r\to 1} D_B^{1-r} \sum_{k=0}^{\infty} \frac{(r/2-1)_k (r)_k}{2^{(k)}} \frac{(2D_B/D_A)^k}{k!}. \tag{5.8}$$

Translating falling factorials to rising factorials with the relation

$$(x)_n = (-1)^n (-x)^{(n)}, \tag{5.9}$$

we arrive at

$$\begin{aligned}\langle D_1^{(2)}(\rho_A, \sigma_A)\rangle &= \lim_{r\to 1} D_B^{1-r} \sum_{k=0}^{\infty} \frac{(-1)^k (1-r/2)^{(k)} (-1)^k (-r)^{(k)}}{2^{(k)}} \frac{(2D_B/D_A)^k}{k!} \\ &= \lim_{r\to 1} D_B^{1-r} \sum_{k=0}^{\infty} \frac{(1-r/2)^{(k)} (-r)^{(k)}}{2^{(k)}} \frac{(2D_B/D_A)^k}{k!},\end{aligned} \tag{5.10}$$

which, in turn, makes the sum readily translated into a hypergeometric function, defined as

$${}_2F_1(a,b,c,z) = \sum_{n=0}^{\infty} \frac{a^{(n)} b^{(n)}}{c^{(n)}} \frac{z^n}{n!}. \tag{5.11}$$

That is,

$$\begin{aligned}\langle D_1^{(2)}(\rho_A, \sigma_A)\rangle &= \lim_{r\to 1} D_B^{1-r} {}_2F_1\left(1-\frac{r}{2}, -r, 2, \frac{2D_B}{D_A}\right) \\ &= {}_2F_1\left(\frac{1}{2}, -1, 2, \frac{2D_B}{D_A}\right).\end{aligned} \tag{5.12}$$

We note that since hypergeometric functions are only defined for $|z| < 1$, the solution above holds only for $D_A > 2D_B$. As expected, we still need to seek for the "other half" of the solution $D_A \leq 2D_B$. Before that, it is noticeable that the result above actually

converges to a much simpler one:

$$\langle D_1^{(2)}(\rho_A, \sigma_A)\rangle = {}_2F_1\left(\frac{1}{2}, -1, 2, \frac{2D_B}{D_A}\right) = 1 - \frac{D_B}{2D_A} = 1 - 2^{N-2N_A-1}, \tag{5.13}$$

where N stands for the total number of qubits in the system and N_A is the number of qubits in subsystem A.

The first half of the solution is obtained by manipulating the initial series (5.5). We can re-write this as

$$\begin{aligned}\langle D_r^{(1)}\rangle &= \lim_{r\to 1}\sum_{k=1}^{r/2}\frac{2^{r/2-k+1}}{r}\binom{r/2}{r/2-k+1}\binom{r}{r/2-k}D_A^{k-r/2}D_B^{1-r/2-k} \\ &= \lim_{r\to 1}\sum_{k=1}^{\infty}\frac{2^{r/2-k+1}}{r}\binom{r/2}{k-1}\binom{r}{k+r/2}D_A^{k-r/2}D_B^{1-r/2-k},\end{aligned} \tag{5.14}$$

where in the first step we made the transformation $k \to r/2-k+1$, and the limits of the sum where switched since in general $r/2 > 1$ (if r is even). In the second step we used that $\binom{n}{k} = \binom{n}{n-k}$ and the upper limit was extended to infinity. As we can see, this new expansion is in powers of $D_A/2D_B$, and thus holds for the first half.

We now follow the same path as before to write the sum as a hypergeometric function

$$\begin{aligned}
\langle D_r^{(1)}\rangle =& \lim_{r\to 1}\sum_{k=1}^{\infty}\frac{2^{r/2-k+1}}{r}\binom{r/2}{k-1}\binom{r}{k+r/2}D_A^{k-r/2}D_B^{1-r/2-k}\\
=& \lim_{r\to 1}\sum_{k=0}^{\infty}\frac{2^{r/2-k}}{r}\binom{r/2}{k}\binom{r}{k+1+r/2}D_A^{k+1-r/2}D_B^{-r/2-k}\\
=& \lim_{r\to 1}\frac{D_A}{r}\left(\frac{2}{D_AD_B}\right)^{r/2}\sum_{k=0}^{\infty}\frac{(r/2)!}{k!(r/2-k)!}\frac{r!}{(k+1+r/2)!(r/2-k-1)!}\left(\frac{D_A}{2D_B}\right)^k\\
=& \lim_{r\to 1}\frac{D_A}{r}\left(\frac{2}{D_AD_B}\right)^{r/2}\sum_{k=0}^{\infty}r!\frac{(r/2-1)!(r/2+1)!}{(r/2-1)!(r/2+1)!}\frac{(r/2)!}{(r/2-k)!}\times\\
&\times\frac{1}{(k+1+r/2)!(r/2-k-1)!}\frac{(D_A/2D_B)^k}{k!}\\
=& \lim_{r\to 1}\frac{D_A}{r}\left(\frac{2}{D_AD_B}\right)^{r/2}\sum_{k=0}^{\infty}\binom{r}{r/2+1}\frac{(r/2)!}{(r/2-k)!}\times\\
&\times\frac{(r/2+2-1)!}{(r/2+2+k-1)!}\frac{(r/2-1)!}{(r/2-1-k)!}\frac{(D_A/2D_B)^k}{k!}\\
=& \lim_{r\to 1}\frac{D_A}{r}\left(\frac{2}{D_AD_B}\right)^{r/2}\binom{r}{r/2+1}\sum_{k=0}^{\infty}\frac{(r/2)_k(r/2-1)_k}{(2+r/2)^{(k)}}\frac{(D_A/2D_B)^k}{k!}\\
=& \lim_{r\to 1}\frac{D_A}{r}\left(\frac{2}{D_AD_B}\right)^{r/2}\binom{r}{r/2+1}\sum_{k=0}^{\infty}\frac{(-1)^k(-r/2)^{(k)}(-1)^k(1-r/2)^{(k)}}{(2+r/2)^{(k)}}\frac{(D_A/2D_B)^k}{k!}\\
=& \lim_{r\to 1}\frac{D_A}{r}\left(\frac{2}{D_AD_B}\right)^{r/2}\binom{r}{r/2+1}{}_2F_1\left(-\frac{r}{2},1-\frac{r}{2},2+\frac{r}{2},\frac{D_A}{2D_B}\right)\\
=& D_A\left(\frac{2}{D_AD_B}\right)^{r/2}\frac{1}{\Gamma(5/2)\Gamma(1/2)}{}_2F_1\left(-\frac{1}{2},\frac{1}{2},\frac{5}{2},\frac{D_A}{2D_B}\right)\\
=& \frac{4\sqrt{2}}{3\sqrt{\pi}}\sqrt{\frac{D_A}{D_B}}{}_2F_1\left(-\frac{1}{2},\frac{1}{2},\frac{5}{2},\frac{D_A}{2D_B}\right).
\end{aligned}\tag{5.15}$$

Gathering results for both halves of the bipartition we then have a complete solution up to corrections small in $1/D$:

$$\langle D_1(\rho_A,\sigma_A)\rangle = \begin{cases} 1-\frac{D_B}{2D_A}, & D_A\geq 2D_B,\\ \frac{8}{3\pi}\sqrt{\frac{D_A}{2D_B}}\,{}_2F_1\left(\frac{1}{2},-\frac{1}{2},\frac{5}{2},\frac{D_A}{2D_B}\right), & D_A\leq 2D_B. \end{cases}\tag{5.16}$$

This stands as the main result of this dissertation, and, as such, it is worthwhile to discuss

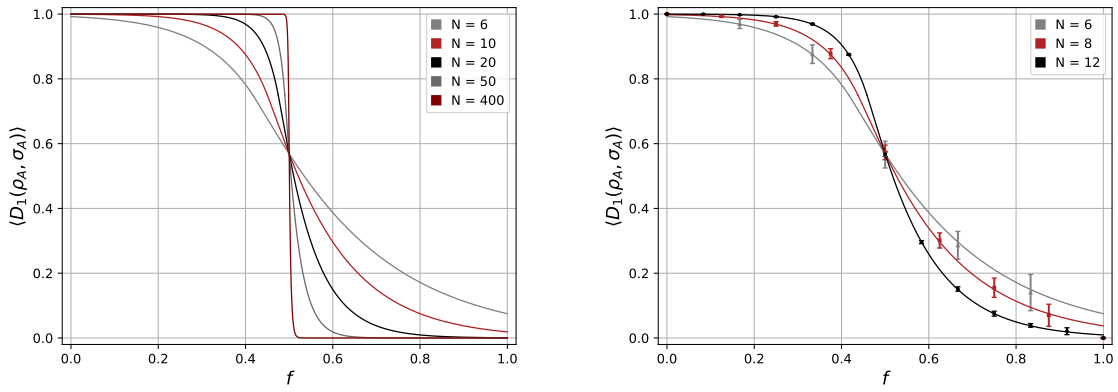

Figure 5.2: Left: Graphics for the main result (5.16) for various system sizes as function of the ratio of unmeasured qubits $f = N_B/N$. We see that as the system increases in size (i.e. in the thermodynamic limit), the trace distance undergoes a first order-like transition from 1 to 0 as half of the qubits are left unmeasured. Right: Comparison between the analytical (5.16) and complete diagonalization simulations for the SYK model, which is fully chaotic, displaying excellent agreement.

it further. In figure 5.2 we see graphics for the result above and its comparison to the SYK model, to excellent agreement. Notably, we chose to plot the trace distance as a function of the ratio of unmeasured qubits $f \equiv N_B/N$ in order to emphasize it as a threshold in the distinguishability between states. Indeed, at $f = 1/2$ we see that a sharp first order-like transition occurs in which we go from $\langle D_1(\rho_A, \sigma_A) \simeq 1$ to $\langle D_1(\rho_A, \sigma_A) \simeq 0$, where '$\simeq$' stands for equality up to corrections small in $1/D$. According to the Holevo-Helstrom theorem (2.6) the optimal probability to distinguish between Page states goes from $P_{\rho\sigma} = 1$ to $P_{\rho\sigma} = 1/2$ in the phase transition as $N \to \infty$. This means that if we measure less than half of the qubits we have no way to distinguish them, and our chances to correctly identify one of two given states reduces to a coin toss, but if we measure more than half we can certainly identify the given state. At $f = 1/2$, i.e. measuring exactly half of the qubits, the optimal probability of distinguishing states is $P_{\rho\sigma} = \frac{5\pi+4}{8\pi} \simeq 0.78$, in agreement with previous work on the subject using free probability calculus in the infinite system size limit Ref. [29]. As a final remark, we note that at $f = 1$ the trace distance is identically zero, as we would be tracing out the whole system, but in figure 5.2 we see that we obtain non-vanishing results in this point, a feature understood if we observe that the Page states as we defined them (4.15) only obey normalization on average, not for single realizations, which leads to the non-zero averaged value we observe.

We can also use both results for the RE of Page states in Eq. (4.52) and the last result

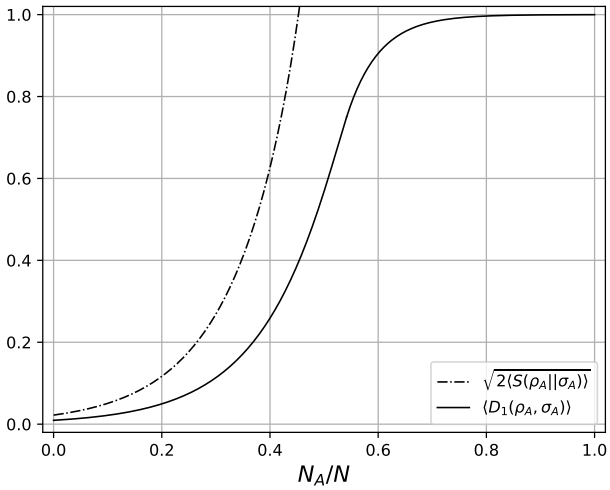

Figure 5.3: Plots for solutions to the square of the relative entropy Eq. (4.52) multiplied by 2 (dash-dotted line) and trace distance Eq. (5.16) (solid line) for Page states of a $N = 12$ qubit system. As we can see, the solutions satisfy Pinkser's inequality Eq. (2.9) (remember that for $N_A > N/2$ the RE is infinite).

for the TD of such states in Eq. (5.16) to verify solutions against Pinsker's inequality Eq. (2.9). In Figure 5.3 we see the comparison of results, satisfying Pinsker's inequality, as expected.

As a final word on Page states, let us quickly evaluate some even Schatten distances, a result we essentially get for free from equation (5.5) by setting r equal to some even number, and one that is not subjected to the analytical continuation performed for $D_1(\rho_A, \sigma_A)$. Below we show the 2- and 4-distances:

$$\begin{aligned}\langle D_2(\rho_A,\sigma_A)\rangle &= \frac{1}{2^{1/2}}||\rho_A-\sigma_A||_2 = \frac{1}{2^{1/2}}(\mathrm{tr}_A(\rho_A-\sigma_A)^2)^{1/2} \\ &= \sqrt{\frac{1}{D_B}} = \sqrt{2^{N_A-N}}\end{aligned} \tag{5.17}$$

$$\begin{aligned}\langle D_4(\rho_A,\sigma_A)\rangle &= \frac{1}{2^{1/4}}||\rho_A-\sigma_A||_4 = \frac{1}{2^{1/4}}(\mathrm{tr}_A(\rho_A-\sigma_A)^4)^{1/4} \\ &= \sqrt[4]{\frac{1}{D_B^3}+\frac{4}{D_A D_B^2}} = \sqrt[4]{2^{3N_A-3N}+2^{N_A-2N+2}}\end{aligned} \tag{5.18}$$

In 5.4 we can see the analytical results for the 2-, 4- and 12-distances against SYK model simulations for a system of $N = 12$ qubits. We can see that as we go to higher n-distances our predictions look increasingly worse as $N_A/N \to 0$. This feature that can be understood by observing that higher distances go with higher powers in $1/D$ [1], meaning

[1] That is, $\langle D_2(\rho_A,\sigma_A)\rangle \sim \mathcal{O}(D^{-1/2})$, $\langle D_4(\rho_A,\sigma_A)\rangle \sim \mathcal{O}(D^{-3/4})$, and so on.

the corrections we neglected by restricting ourselves to non-crossing partitions would be more relevant for those cases as $N_A/N \to 0$.

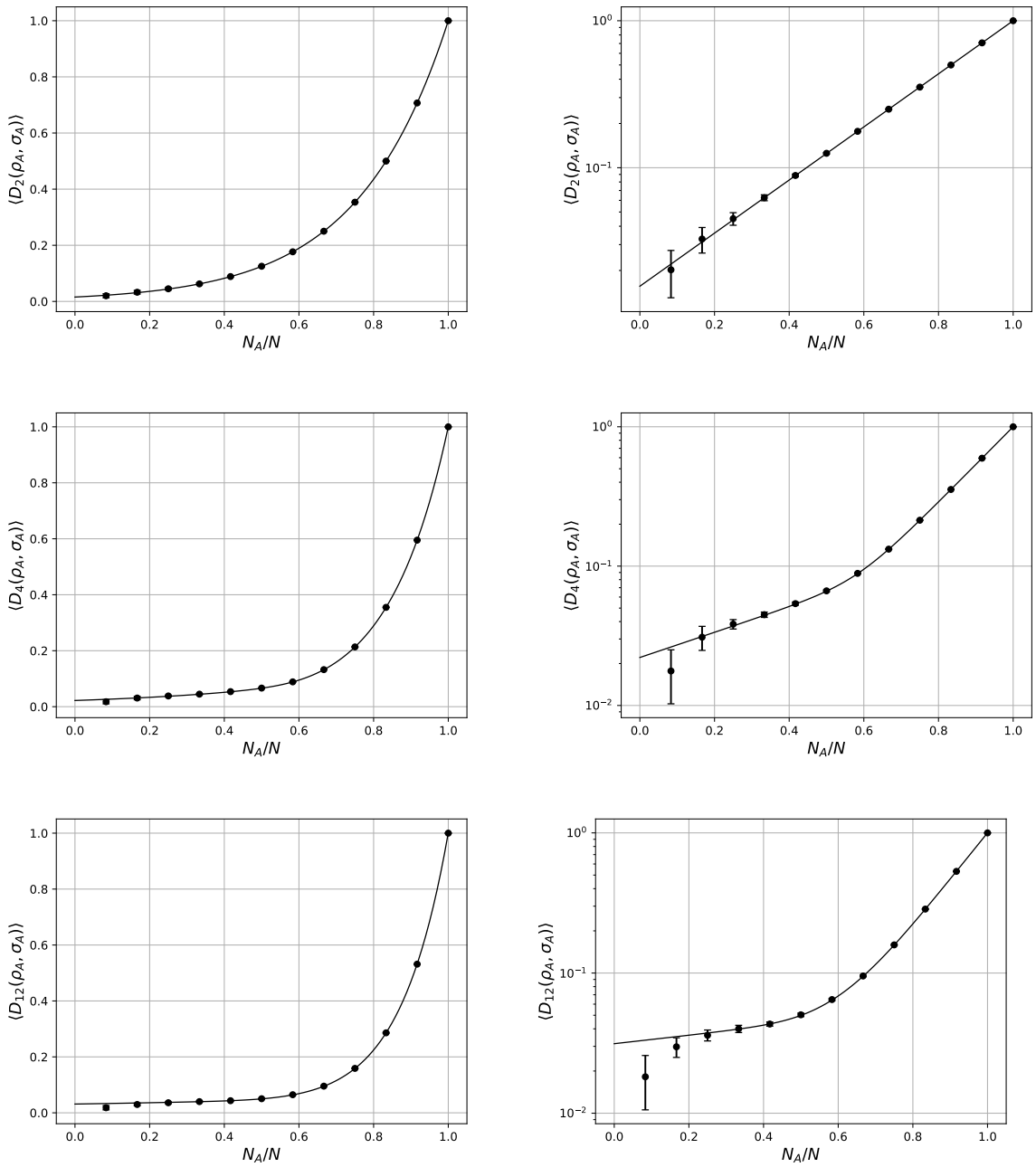

Figure 5.4: All Graphs are numerical results of Schatten n-distances for simulations of SYK model states accompanied by their analytical prediction. The graphs in the left are simply the ones in the right presented in logarithmic scale. From top to bottom, we present the Schatten 2-, 4- and 12-distances, respectively.

5.2 Trace Distance (TD) - Systems with Conservation Laws

We next discuss the impact of local conservation laws on the TD. To this end we build on the formalism of previous sections, in the same lines as the treatment of the EE for systems with conservation laws. The change that must be made in the derivation of an equation for the TD for Page states is in the Gaussian variance of the amplitudes, which now follows (4.6). As before, we will employ a replica-trick that requires the evaluation of the moments $M_r'' \equiv \mathrm{tr}_A([\rho_A - \sigma_A]^r)$ and our previous discussion on the combinatorial structure of said moments mostly holds here too, with a translation for states with conservation laws done as for the EE using the relation (4.21). This leads us to:

$$\begin{aligned}\mathrm{tr}_A([\rho_A-\sigma_A]^r) =& \frac{1}{D^r\Omega^r(Q)}\sum_{k=1}^{r/2}\frac{2^{k+1}}{r}\binom{r/2}{k}\binom{r}{k-1}\sum_{Q_A}D_A^{r-k+1}\Omega_A^{r-k+1}(Q_A)D_B^k\Omega_B^k(Q-Q_A)\\ =&\sum_{k=1}^{r/2}\frac{2}{r}\binom{r/2}{k}\binom{r}{k-1}\sum_{Q_A}\frac{F_A^{r+1}(Q_A)}{F^r(Q)}\left(\frac{2F_B(Q-Q_A)}{F_A(Q_A)}\right)^k.\end{aligned} \tag{5.19}$$

This introduces a new cutoff: We have to treat the regions $2F_B(Q-Q_A) < F_A(Q_A)$ and $2F_B(Q-Q_A) > F_A(Q_A)$ separately, and now we cannot simply take the second part of the solution as a trivial $(A \leftrightarrow B)$ substitution like we did with the EE. We have dealt with the structure above in our earlier treatment of the trace distance for Page states. If we note that the manipulations following (5.5) through (5.16) deal with the index k from the combinatorics and that there is a one-to-one correspondence between D_S and $F_S(Q_S)$ connecting the scenarios, we can recycle the calculation (the main difference is that now we must keep $F^r(Q)$ factored out, while we cancelled D^r against D_A and D_B factors previously). This procedure leads us to:

$$\begin{aligned}\langle D_1(\rho_A,\sigma_A)\rangle =& \frac{1}{F(Q)}\sum_{Q_AQ_B}\left\{\left(F_A(Q_A)F_B(Q_B)-\frac{1}{2}F_B^2(Q_B)\right)\Theta_<+\right.\\ &\left.+\frac{4\sqrt{2}}{3\pi}F_A^{3/2}(Q_A)F_B^{1/2}(Q_B){}_2F_1\left(-\frac{1}{2},\frac{1}{2},\frac{5}{2},\frac{F_A(Q_A)}{2F_B(Q_B)}\right)\Theta_>\right\}\delta_{Q,Q_A+Q_B},\end{aligned} \tag{5.20}$$

where $\Theta_< \equiv \Theta(F_A(Q_A) - 2F_B(Q_B))$ and $\Theta_> \equiv \Theta(2F_B(Q_B) - F_A(Q_A))$.

Focusing on the peak of the DoS we fix $Q = 0$, as done for the EE in the previous section. We saw how this allowed us to switch $\Theta(F_B(Q_B) - F_A(Q_A))$ for a friendlier $\Theta(N_B - N_B)$ by inspecting the behaviour of the derivatives of spectral distributions with respect to the number of qubits in subsystem A. The monotonic increase (decrease) of $F_A(Q_A)$ ($F_B(Q_B)$) as N_A increases still holds, and we must look for the point where the $F_A(Q_A) = 2F_B(Q_B)$. At $N_A = N_B = N/2$ it is obvious that $F_A(Q_A, N_A = N/2) < 2F_B(Q_B, N_B = N/2)$. However, at least in the large N limit, we also have $F_A(Q_A, N_A = N/2 + 1) > 2F_B(Q_B, N_B = N/2 - 1)$. This means that the transition in the Heaviside step-functions occurs at a non-integer value for N_A (N_B) between $N_A = N/2$ ($N_B = N/2$) and $N_A = N/2 + 1$ ($N_B = N/2 - 1$). Since our physical system must have an integer number of qubits we can stick to translation $\Theta(F_B(Q_B) - F_A(Q_A)) \to \Theta(N_B - N_B)$ with impunity. This makes it simple to evaluate the equation above. By approximating the sum over Q_A as an integral again we can show that

$$\frac{1}{F(0)} \sum_{Q_A} F_A^k(Q_A) F_B^m(-Q_A) = \frac{D_A^k D_B^m}{(2\pi\gamma^2)^{\frac{k+m}{2}-1} D} \sqrt{\frac{N_A N_B}{N_A^k N_B^m}} \sqrt{\frac{N}{mN_A + kN_B}}. \tag{5.21}$$

Using this we arrive at (we write the hypergeometric function as its defining sum form for the calculation),

$$\langle D_1(\rho_A, \sigma_A) \rangle = \begin{cases} 1 - \frac{D_B}{2D_A}\sqrt{\frac{N}{2N_B}} & D_A \geq 2D_B, \\ \sum_{k=0}^{\infty} \sqrt{\frac{4N}{(1+2k)N_B + (1/2-k)N}} \left(\frac{D_A}{2D_B}\sqrt{\frac{N_B}{N_A}}\right)^{k+\frac{1}{2}} \binom{1/2}{k} \binom{1}{k+3/2}, & D_A \leq 2D_B. \end{cases} \tag{5.22}$$

In Figure 5.5 we show two plots illustrating the above result. On the left we see the comparison between the TD of Page states (5.16) and charge eigenstates at the peak of the DoS (5.22). Firstly, we note that the best success probability for discriminating states (given by (2.6)) for charge eigenstates is smaller than for Page states for $f < 1/2$ and bigger for $f > 1/2$. This supports the notion that the charge conservation constrains the Hilbert space 'available' to states: if we trace out less than half the qubits, charge eigenstates occupying a smaller space are less distinguishable. However, as we trace out more than half of the qubits, Page states loose more information, as they loose a

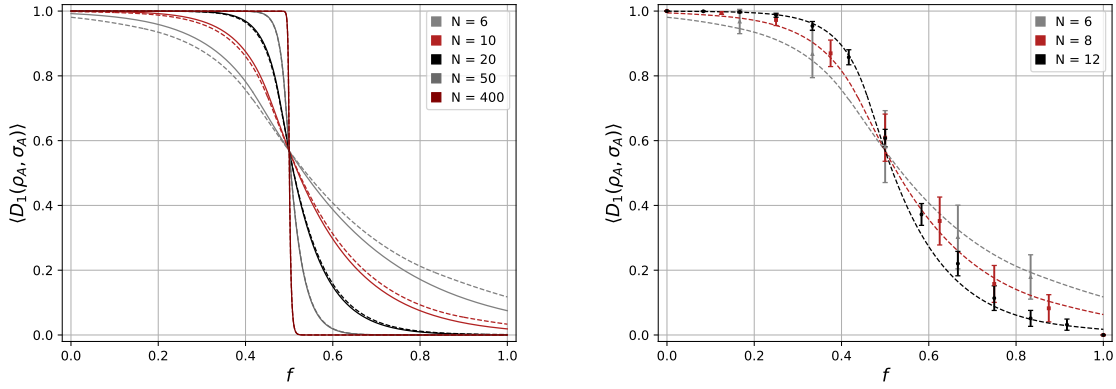

Figure 5.5: Left: Plots for the average trace distance for Page states (5.16) (solid lines) and charge eigenstates near $Q = 0$ (5.22) (dashed lines) as function of the fraction of traced out qubits $f \equiv N_B/N$ (extremes of the plot are interpolations as discussed in the main text). Right: Comparison between the analytical prediction (5.22) and simulations for a spin-1/2 Ising chain with longitudinal and transversal fields (see 6). We average over pairing of the 7 states closest to the peak of density of states.

larger fraction of their Hilbert space, and thus become less distinguishable. Secondly, the differences between TDs of both set of states become less notable as the system size increases. Said differences are most pronounced as $f \to 1/N$ and $f \to 1 - 1/N$. Also, note that (5.22) diverges in the limits $f = 0$ and $f = 1$, where F_B and F_A become delta-functions, respectively. Thus, for these points we must turn back to equation (5.20) and take $F_B = 1$ and $F_A(Q_A) = F(Q)$ at $f = 0$ and $F_A = 1$ and $F_B(Q_B) = F(Q)$ at $f = 1$ for a sensible result, which we use to interpolate (5.22) using a quadratic polynomial. Finally, we note that at half-partition, $f = 1/2$ the results for Page states and charge eigenstates with largest spectral weight actually become identical, which contrasts with the result for the EE, which shows the largest deviation between both set of states at half-partition. In the left plot of Figure 5.5 we see the analytical prediction above against numerical simulation of a system that should follow it, a spin 1/2 Ising chain with longitudinal and transversal fields (see Chapter 6 for more details). We see good agreement with the prediction, however not as great as for the SYK model, which perfectly followed Page states. Deviations can be attributed the charge eigenstates not having $E = 0$, being away from the peak of the density of states due to system size limitations and deviations of the DoS itself from the Gaussian profile of Eq. (4.27). Still, we have good agreement for small system sizes, with Hilbert space dimensions as small as $D = 2^6$.

As a final exploration of the TD, let us explore its behaviour for finite charges close

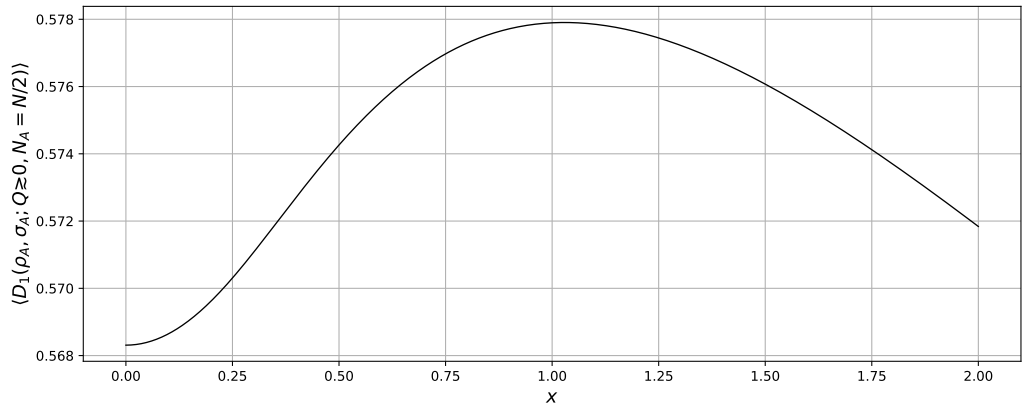

Figure 5.6: Trace distance between charge eigenstates at half partition, as described by equation (5.24). The TD is plotted as a function of $x \equiv Q/\gamma\sqrt{N}$. As one can see it reaches a maximum at $Q = \gamma\sqrt{N}$.

to the peak fixed at $Q = 0$. Here we choose to focus on half partitions $N_A = N_B = N/2$, as well as the limits $f \to 1/N$ and $f \to 1 - 1/N$. At half partition, the summations of the type of the ones in (5.20) can be worked to yield,

$$\begin{aligned}\frac{1}{F(Q)}\sum_{Q_A} F_A^k(Q_A)F_B^m(Q-Q_A)\Theta_{>/<} =& \frac{D_A^k D_B^m}{D}\frac{\sqrt{2\pi\gamma^2 N}}{(\pi\gamma^2 N)^{\frac{k+m}{2}}} e^{-\frac{2km-k-m}{k+m}\frac{Q^2}{2\gamma^2 N}}\times \\ &\times \sum_{Q_A} e^{-\frac{(k+m)Q_A^2}{\gamma^2 N}}\theta_{>/<}\left(Q_A + \frac{m}{k+m}Q\right),\end{aligned} \tag{5.23}$$

where $\theta_<(Q_A + \frac{m}{k+m}Q) \equiv \theta(Q/2 - \frac{NC}{2Q} - \frac{m}{k+m}Q - Q_A)$, $\theta_>(Q_A + \frac{m}{k+m}Q) \equiv \theta(Q_A - Q/2 + \frac{NC}{2Q} + \frac{m}{k+m}Q)$, and $C \equiv \gamma^2 \ln 2$. Using this result in (5.20) with arrive at the following expression for the trace-distance at half partition,

$$\begin{aligned}\langle D_1(\rho_A, \sigma_A)\rangle =& \frac{1}{2}\,\mathrm{Erfc}\left(\sqrt{\frac{N}{2\gamma^2}}\frac{C}{Q}\right) - \frac{1}{4}e^{\frac{Q^2}{2\gamma^2 N}}\,\mathrm{Erfc}\left(\frac{NC+Q^2}{Q\sqrt{2\gamma^2 N}}\right) \\ &+ \sum_{k=0}^{\infty}\binom{1/2}{k}\binom{1}{k+3/2}\left[\frac{e^{\frac{(k+1/2)Q^2}{2\gamma^2 N}}}{2}\right]^{k+1/2}\mathrm{Erfc}\left(\frac{(1+2k)Q^2 - 2NC}{2Q\sqrt{2\gamma^2 N}}\right),\end{aligned} \tag{5.24}$$

where $\mathrm{Erfc}(x) = (2/\sqrt{\pi})\int_x^\infty e^{-t^2}dt$. We can solve this numerically, resulting in the plot in Figure 5.6. As we can see in the figure the equation above predicts that the TD

at half partition increases with Q up to $Q = \gamma\sqrt{N}$, when it reaches ~ 0.578, and then decreases. As Q increases, the solution seems to converge to $Q = 0.5$, but we do not expect predictions for large Q to remain valid as specific properties of the spectral distribution become more relevant and the Gaussian assumption becomes invalid.

Finally, we evaluate some limits of the distribution for finite Q. For $f \to 1/N$ we neglect the $\Theta_>$ contribution in (5.20), and find $\langle D_1 \rangle \approx 1 - \sqrt{N} e^{-Q^2/2\gamma^2 N}/D$, and the leading contribution for $f \to 1 - 1/N$, neglecting the $\Theta_<$ term, is $\langle D_1 \rangle \approx N^{1/4} e^{Q^2/4\gamma^2 N}/\sqrt{D}$. Both these results correspond to substitutions of the type $D_S \mapsto F_S(Q)$ in equation (5.16) for Page's states. This results corroborates the interpretation in which charge eigenstates' phase spaces are reduced in volume relative to Page's.

5.3 Summary

We have managed to develop fully analytical results for the trace distance of random states of systems without Eq. (5.16) and with Eq. (5.22) local conservation laws. These are the main results of our work. It is interesting to consider them as it pertains the ETH and subsystem ETH presented in chapter 1. We have considered the average trace distance of eigenstates of qubit systems after restricting to a subsystem A by tracing out a fraction N_B/N of qubits. Our results show that our chances of correctly distinguishing between two random states with an optimally chosen experiment, as encoded in the trace distance via the Holevo-Helstrom theorem Eq. (2.6), is directly linked to the relative size of subsystem A in relation to the full system. If $N_A > N/2$ we can correctly distinguish states, but if $N_A < N/2$ distinguishing states becomes hopeless, with accuracy reducing to a coin flip. This establishes a clear boundary for distinguishability in the thermodynamic limit. Notably, although the presence of locally conserved charges introduces some corrections in relation to the systems without conserved charges, this behaviour is still observed for those systems in the thermodynamic limit.

This results gives us plenty of insight into the validity of the subsystem ETH. According to this postulate, as we consider a small enough subsystem A by tracing out the rest of a larger system, the density matrix associated with it is exponentially close to an universal density matrix depending smoothly on the energy of the system. This readily links to our findings. Here, a 'small enough' subsystem A is a system with $N_A < N/2$ qubits, where

distinguishability of eigenstates is impossible. In this region, all states 'look the same', being described the universal thermal density matrix postulated by the subsystem ETH. Our results then corroborate the subsystem ETH, which strengthens the usual ETH by postulating that moments of the density matrix themselves appear thermal, rather than few-body observables as postulated by the latter.

Chapter 6

Models and simulations

Throughout the dissertation so far, we have managed to derive several analytical results describing entanglement properties of ergodic states under different partitions. Those results were corroborated by simulations that showed good to excellent agreement with analytical calculations, providing support for all assumptions made. Little has been said about these simulations however, and this chapter focuses on elucidating them. We begin the chapter by presenting the procedure used for computing entanglement properties, via single value decomposition. Then, we go over to the models describing ergodic quantum systems, with and without local conservation laws. All codes were written in python, but we here choose not to go into details as they present no innovative aspect.

6.1 Procedure

All simulations are carried out by exact diagonalizing of Hamiltonians. Here we go over the procedure for analysing the eigenstates obtained from diagonalization, and the computation of the entanglement properties of interest.

All computational procedures were based on the use of singular value decomposition (SVD). We found this method both the most efficient and instructive (this illustrates perfectly why the RE is infinite for $N_A > N_B$).

According to equation (4.2), we can write the most general density matrix associated to a pure state as

$$\rho = \sum_{a,b} \sum_{a',b'} \psi_{ab} \bar{\psi}_{a'b'} \left|a, b\right\rangle \left\langle a', b'\right| . \tag{6.1}$$

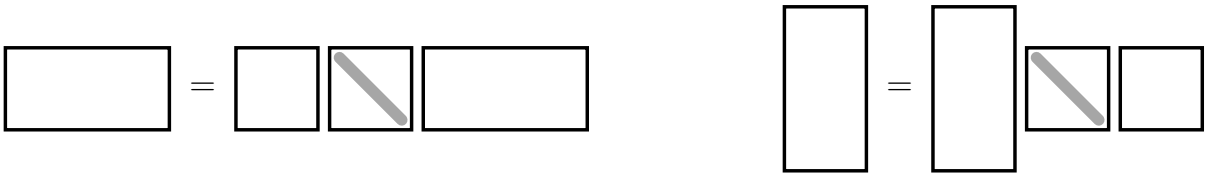

Figure 6.1: Diagrams that show the shapes of the matrices U, S and $V^\dagger$ in equation (6.4), respectively. Left: case in which $\dim A < \dim B$. Right: case in which $\dim A > \dim B$. Shaded region indicates matrices that are diagonal.

The reduced density matrix associated to subsystem A is then:

$$\rho_A = \mathrm{tr}_B\, \rho = \sum_{a,a'} \left[\sum_b \psi_{ab} \bar{\psi}_{a'b} \right] |a\rangle \langle a'| \,. \tag{6.2}$$

Now, if we define a matrix Ψ whose elements are defined as $[\Psi]_{ab} \equiv \psi_{ab}$, we can write:

$$\rho_A = \Psi \Psi^\dagger. \tag{6.3}$$

According to the SVD theorem, we can decompose Ψ as

$$\Psi = USV^\dagger, \tag{6.4}$$

where U and V are unitary matrices and S is a diagonal matrix whose elements $S_{\alpha\alpha} = \sigma_\alpha$ are called singular values and are real. Now, the indices a and b run through the subspaces of a Hilbert space that not necessarily are of the same dimension, meaning that Ψ is, in general, a rectangular matrix. In fact, a quick inspection of the equation (6.4) above shows that shapes of U, S and V are such as illustrated in Figure 6.1.

Using the decomposition above we can write

$$\rho_A = \Psi \Psi^\dagger = USV^\dagger VSU^\dagger = US^2U^\dagger. \tag{6.5}$$

It is clear, since S is diagonal and U is unitary, that comparing the expression above with a diagonalization of ρ_A we can establish U as the matrix whose columns are eigenvectors of ρ_A and the singular values of S are related to the eigenvalues of ρ_A through

$$\sigma_\alpha^2 = \lambda_\alpha. \tag{6.6}$$

Now, we can also write

$$\Psi^\dagger\Psi = VSU^\dagger USV^\dagger = VS^2V^\dagger, \tag{6.7}$$

which gives us another diagonalization, this time of the matrix $\Psi^\dagger\Psi$. We can readily see that matrices $\Psi\Psi^\dagger$ and $\Psi^\dagger\Psi$ share the same eigenvalues of S^2, but also that these matrices have, when Ψ is rectangular, different shapes, meaning the bigger one of the two will have the same eigenvalues of the smaller one plus a bunch of zero eigenvalues. In fact, since the elements of Ψ are ψ_{ab} and $\rho_A = \Psi\Psi^\dagger$, we see that when $\dim A > \dim B$, ρ_A necessarily has at least one of its eigenvalues equal to zero.

A python routine readily evaluates the matrices of the SVD. Let us see how the entanglement properties are defined in terms of those matrices.

The EE is the most straightforward of the bunch. We have:

$$S(\rho_A) = -Tr(\rho_A \ln \rho_A) = -\sum_\alpha \lambda_\alpha \ln \lambda_\alpha = -\sum_\alpha \sigma_\alpha^2 \ln \sigma_\alpha^2, \tag{6.8}$$

and we need only the elements of S to evaluate it.

For the RE we also will need to use the U matrix. Given two density matrices ρ_A and σ_A:

$$S(\rho_A||\sigma_A) = -\operatorname{tr}(\rho_A \ln \sigma_A) - S(\rho_A) = -\operatorname{tr}\Big(U_\rho S_\rho^2 U_\rho^\dagger U_\sigma [\ln S_\sigma^2] U_\sigma^\dagger\Big) - S(\rho_A). \tag{6.9}$$

In the equation above we can see why the RE is infinite for $\dim A > \dim B$. In that case, we have already seen that both matrices will necessarily have zero eigenvalues. This presents a problem because the evaluation of $\ln S_\sigma^2$ will have a term "$\ln 0$" which is equal to $-\infty$. This does not pose a problem to the evaluation of the EE, because for the EE the logarithm of the eigenvalue is multiplied by that eigenvalue and we set $0 \ln 0 = 0$, which is justified by $\lim_{x\to 0} x \ln x = 0$. For the RE however we cannot assure that $\ln 0$ is multiplied by zero because it is not true that $U_\rho^\dagger U_\sigma = I$ since ρ_A and σ_A are not simultaneously diagonalizable in general. This is why we restricted ourselves to the cases $N_A \leq N/2$ in the sections on RE.

Now let us turn to the TD. It too is calculated via SVD. Following its definition

$$D_1(\rho,\sigma) = \frac{1}{2}||\rho - \sigma||_1, \tag{6.10}$$

where

$$||\Lambda||_n = \left(\sum_i \lambda_i^n\right)^{1/n}, \tag{6.11}$$

and λ_i are the eigenvalues of $\sqrt{\Lambda^\dagger \Lambda}$, we can directly evaluate:

$$D_1(\rho,\sigma) = \frac{1}{2}||U_\rho S_\rho^2 U_\rho^\dagger - U_\sigma S_\sigma^2 U_\sigma^\dagger||_1. \tag{6.12}$$

Now that we have gone through a quick exposition on the algorithms for computing the entanglement properties via the SVD, let us look at the actual models employed to support the analytical findings of the previous chapters.

6.2 SYK model

As an ergodic system with no conservation laws we choose to work with the Sachdev-Ye-Kitaev (SYK) model. The states of this system should behave as Page states, i.e. are random vectors Haar-distributed across the entire Hilbert space of a N-qubit system. The Hamiltonian for this system is [10, 11]:

$$\hat{H}_{SYK} = \frac{1}{4!}\sum_{i\leq j\leq k\leq l}^{2N} J_{ijkl}\chi_i\chi_j\chi_k\chi_l, \tag{6.13}$$

where $\{\chi_i\}$ are Majorana operators:

$$\{\chi_i, \chi_j\} = \delta_{ij}, \tag{6.14}$$

and the entries in the tensor J_{ijkl} are random Gaussian distributed variables obeying

$$\langle J_{ijkl}\rangle = 0, \qquad \langle J_{ijkl}^2\rangle = \frac{3J^2}{4N^3}. \tag{6.15}$$

Also, the tensor J_{ijkl} must be anti-symmetrical over any index permutation to guarantee hermiticity. The variable J controls thus the energy scale of the system, and we fix it to $J = \sqrt{2/N}$. This should not matter much since we will not be considering any other term

in the Hamiltonian to compete with the ergodic one above.

The above system of $2N$ Majorana fermions present a one-to-one correspondence with a system of N conventional fermions via the transformations

$$c_i = \frac{1}{2}(\chi_{2i-1} + i\chi_{2i}), \qquad c_i^\dagger = \frac{1}{2}(\chi_{2i-1} - i\chi_{2i}). \tag{6.16}$$

Crucially, when performing the transformations above, the terms $\chi_i\chi_j\chi_k\chi_l$ in the Hamiltonian yield many terms, including familiar ones like $c_i^\dagger c_j^\dagger c_k c_l$ but also ones like $c_i^\dagger c_j^\dagger c_k^\dagger c_l$. The last one of those correspond to the annihilation of a fermion followed by the creation of three others, which exemplifies the core featured we are interested, this system does not conserve any charge or particle number locally. In fact, the only symmetry present is a fermion parity symmetry, which can be avoided by restricting analysis to a fixed parity sector[1]. This means that for simulating a N qubit system one must work with a SYK model with $N+1$ fermions ($2N+2$ Majorana fermions), and after diagonalizing the Hamiltonian, work with eigenstates of fixed fermion parity (either odd or even), whose Hilbert space is of dimension 2^N.

Now, let us see why we may label the states of the SYK model above as *ergodic*. Ergodicity is established if the eigenstates are uniformly distributed over the Hilbert space available to the system, which in this case is a 2^N-dimensional hypersphere. This can be verified by checking if the wavefunction distribution of the systems follows the Porter-Thomas distribution for the Gaussian Unitary Ensemble (see discussion on Random Matrix Theory in Chapter 1):

$$P_{GUE}(y) = e^{-y}, \tag{6.17}$$

where $y = D|\psi_n|^2$, and ψ_n are the amplitudes of the eigenvector $|\psi\rangle$ of the Hamiltonian with fixed parity (here D is the dimension of a parity sector of the Hamiltonian). In Figure 6.2 we see the comparison of the statistics of eigenstates of the SYK model with $N = 11$ fermions (after restricting to the even sector this corresponds to an $N = 10$ qubit system), which displays excellent agreement, confirming the ergodicity of the system.

Since we established the procedure for computing entanglement properties in the pre-

[1]Since the each term in the Hamiltonian contains an even number of fermionic creation/annihilation operators, the overall Hamiltonian preserves parity of fermionic states. Thus, we can diagonalize the Hamiltonian in two sectors, with even and odd parity which do not interact with each other.

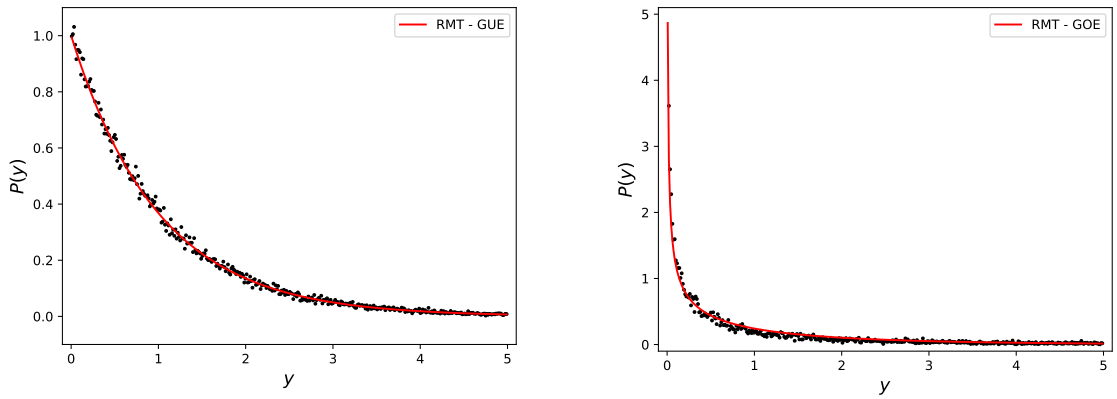

Figure 6.2: In both plots black dots show the statistical distribution of the normalized intensities $y = D|\psi_n|^2$ of 20 eigenstates of ergodic systems and the red curve shows the prediction from RMT for the corresponding symmetry class, given by the Porter-Thomas distributions in Eq. (1.5). In both cases we chose eigenstates at the peak of the density of states. Left: SYK model with $N = 13$ fermions (thus $D = 2^{12}$), described by the GUE. Right: Spin Chain system with $N = 12$ spins described by the GOE.

vious section, it is clear how to carry out simulations once we get eigenstates of the SYK Hamiltonian by exact diagonalization. As for specific aspects of the simulation, we point that states are taken from the peak of the density of states, at zero energy, and that all plots in previous chapters are averaged over 50 samples of J_{ijkl} realizations.

As a final word on these states, we merely note that we expect eigenstates of the SYK model to be statistically equivalent to simply drawing random states:

$$|\psi\rangle = \sum_{a,b} \psi_{a,b} \, |a, b\rangle \tag{6.18}$$

with $\psi_{ab} = re^{i2\pi\theta}$, where r and θ are randomly selected from a uniform distribution of $[0, 1)$ and normalizing the state afterwards. The choice of working with the SYK system aims at providing a better support to the idea that such states, as simple as they look, are not as artificial and void of physical significance as one may think.

6.3 Spin Chain

For an ergodic system with a locally conserved charge we choose to work with an spin-1/2 Ising chain with nearest neighbour interaction in presence of a longitudinal and transversal magnetic field [12, 13, 14]:

$$\hat{H}_S = \sum_{i=1}^{N} (g\hat{\sigma}_i^x + h\hat{\sigma}_i^z + J\hat{\sigma}_i^z\hat{\sigma}_{i+1}^z), \tag{6.19}$$

where $\{\hat{\sigma}_i^x, \hat{\sigma}_i^z\}$ are Pauli matrices and we work with periodic boundary conditions, $\sigma_{N+1} = \sigma_1$. The parameters of the Hamiltonian are set to $(g, h, J) = (0.9045, 0.8090, 1.0)$, for which the system is known to be thermalizing for small system sizes [12, 13, 14]. We also check ergodicty by comparing the wavefunction statistics of the system with the prediction for the Gaussian Orthogonal Ensemble from RMT given by:

$$P_{GOE}(y) = \frac{1}{\sqrt{2\pi y}} e^{-\frac{y}{2}}. \tag{6.20}$$

In Figure 6.2 we see the comparison of the above prediction with a $N = 12$ spin chain, finding good agreement.

Now, since the Hamiltonian for the system is translational invariant we must block diagonalize in momentum sectors, which thermalize independently. We here restrict to the zero-momentum sector, the largest, and within it only energy is conserved. Notice here that, in contrast with the SYK model, parameters are fixed and no averages over realizations can be performed. Then, we pick a few states with energies around the peak of the density of states to average over (specified in each plot). This limits the accuracy of our simulations, as we are already working within a relatively small Hilbert space due the restricting to a given momentum sector. Thus, some states we take for the statistical average are farther from the peak of the DoS, and their behaviour might not follow the model (4.27) as closely. We point to this as the main source of deviations in the results in Figure 4.3 and Figure 5.5.

In order to select which eigenstates we take for the simulation, we begin by calculating the density of states of the system. From it, we can determine the peak of the density states, and choose a few states with energies centred around it. All these steps are taken after fixing the momentum sector. In Figure 6.3 we illustrate this procedure in the inset. Figure 6.3 is for a chain of 10 spins, for which we find the DoS to be reasonably described by a Gaussian with peak localized at -0.4 ± 0.3. For the TD displayed in the figure we take 5 eigenstates from the window $\sim (-0.8, 0.0)$. As we can see, we get good results, but the statistics is not large, and better results comes down to fine tuning the set of states taken around the peak since we can't simply average over parameters. See Appendix B

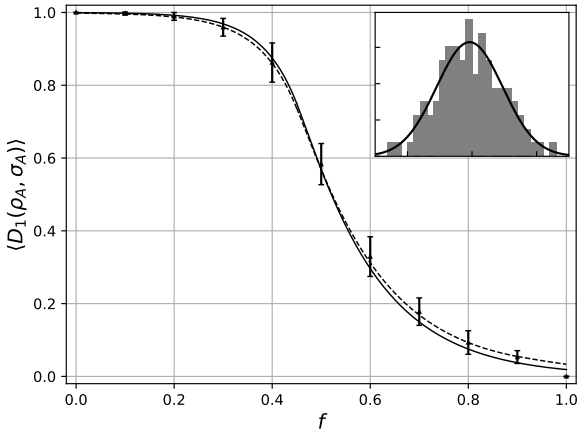

Figure 6.3: Subsystem trace-distances from exact diagonalization for a chain of 10 spins. Solid and dashed lines are the analytical predictions in absence (5.16), and presence of conservation laws (5.22). Inset: Density of states for zero momentum eigenstates with Gaussian fit (solid line).

for a more in depth look at some of the aspects discussed here.

Chapter 7

Conclusion

This work aims to develop a better understanding of ergodic states both with and without the presence conservation laws. To this end, we explored entanglement properties of such states upon bi-partitioning, which encode much of the distribution of information and possibilities of distinguishing between them. We thus employed minimal models for the structure of ergodic states with and without conservation laws by assuming vectors with random Gaussian amplitudes with zero mean and proper variance. This simple, yet fairly general model, enabled us to find analytical predictions for the behaviour of the entanglement entropy, relative entropy (for states without conservation laws) and the trace distance of such states upon bi-partitioning of the system. All results were checked against exact diagonalization of ergodic systems we expect to model with our approach.

The entanglement entropy has been of random states has been largely explored in the literature (e.g. [7, 3]), with fully analytical solutions for both Page states and eigenstates of system with local conservation laws. The relative entropy has also seen a complete treatment in Ref. [8]. For the trace distance, even though some interesting results have been found [9], had not seen a fully analytical solution similar to the ones for the EE and RE, to the best of our knowledge. We here provided such solution for both Page states and eigenstates of systems with conservation laws. In the table above we gather all results developed for ergodic states with and without conservation laws and present them in a compact notation:

	Page states	Systems with local conserved charge
$\langle S(\rho_A)\rangle$	$\ln D_A - x$	$\ln D_A - \frac{1}{2}\ln\frac{1}{f} + \frac{1-f}{2} - \sqrt{\frac{1}{2(1-f)}}x$
$\langle S(\rho_A\|\|\sigma_A)\rangle$	$1 + \left(\frac{1}{2x} - 1\right)\ln(1-2x) + x$	-
$\langle D_1(\rho_A, \sigma_A)\rangle$	$\begin{cases} 1 - \frac{1}{4x}, & x \geq 1, \\ \frac{8\sqrt{x}}{3\pi}\mathcal{F}(x), & x \leq 1, \end{cases}$	$\begin{cases} 1 - \frac{1}{4x\sqrt{2f}}, & x \geq 1, \\ \frac{8\sqrt{x_f}}{3\pi}\mathcal{G}(x_f, f), & x \leq 1, \end{cases}$

where $f = N_B/N$, $x = \frac{D_A}{2D_B}$, $x_f \equiv x\sqrt{f/(1-f)}$, $\mathcal{F}(x) = {}_2F_1(\frac{1}{2}, -\frac{1}{2}, \frac{5}{2}, x)$ is a hypergeometric function and $\mathcal{G}(x, f) = \frac{3\pi}{4}\sum_{k=0}^{\infty} c_k x^k \binom{1/2}{k}\binom{1}{k+3/2}$ with $c_k = ((1+2k)f + 1/2 - k)^{-1/2}$.

Our main results Eq. (5.16) and Eq. (5.22) together with the Holevo-Helstrom theorem Eq. (2.6), show that the distinguishability of ergodic states by measuring a fraction of the whole system, in the thermodynamic limit, is directly linked to whether we measure more or less than half of the systems overall degrees of freedom. That is, a sharp first order-like transition occurs in which the probability of correctly identifying one of two given states is ~ 1 if we measure more than half of the qubits of a system, but ~ 0 if we measure less than half. This can be thought of as a self-averaging transition $\rho \to \langle\rho\rangle$ for $N_B > N/2$. Moreover, we verified this behaviour holds as we introduce conservation laws to the system, with deviations only relevant at small system sizes. Also, we verified Pinsker's inequality Eq. (2.9) using our results for the trace distance Eq. (5.16) and the relative entropy Eq. (4.52) of Page states.

Our main interest in these states is related to the eigenstates thermalization hypothesis and the characterization of chaotic dynamic limits in quantum mechanics. In trying to describe how isolated quantum systems thermalize, the ETH argues that information scrambling acts as to make subsystems of the original system behave as if connected to thermal reservoirs. However, if we can distinguish between two subsystem realizations we cannot claim thermal behaviour to be attained, thus the trace distance provides us with the upper boundary for how small subsystems must be in order to be described by the ETH, i.e. they must be at most half the systems' original 'size'. In fact, our findings corroborate an even stronger postulate for thermalization, the subsystem ETH. By states themselves becoming indistinguishable we support the notion that the density matrices of such systems look thermal. This is constrains significantly the original postulate of the ETH in which only expectation values of observables look thermal.

We conclude with some remarks on possible works in the future. One interesting route

may be the exploration of other moments for the entanglement properties discussed here. Here we focused on the averages, but evaluating e.g. the variance we may develop an understanding on the fluctuations of results obtained. Another path concerns systems that elude thermalization and chaotic behaviour, such as many-body localized regimes, where we would like to better understand the breakdown of the ETH.

Appendix A

Distribution of States

Here we introduce a very important tool for the analytical calculations done in this work, the distribution of states (DoS). Given an operator $\hat{Q}$ associated with a set of conserved quantities of the system, the DoS for a set of fixed values Q of said quantities is

$$D\Omega(Q) = \mathrm{tr}_S(\delta_{\hat{Q},Q}), \tag{A.1}$$

where D is the dimension of the Hilbert space we are looking at, and $S = A, B$. Also

$$\delta_{\hat{Q},Q} = \prod_{k=1}^{M} \delta_{\hat{q}_k,q_k}, \tag{A.2}$$

where indices $k = 1, 2, ..., M$ label the conserved quantities of the system.

Now, the canonical partition function can be obtained by taking the Laplace transform of the DoS

$$Z(\beta_Q) = \sum_Q \Omega(Q) e^{-\beta_Q Q}. \tag{A.3}$$

If we assume that the system is described by a canonical equilibrium density matrix

$$\rho(\beta_Q) = \frac{e^{-\beta_Q \hat{Q}}}{Z(\beta_Q)}, \tag{A.4}$$

with partition function:

$$Z(\beta_Q) = \mathrm{tr}\, e^{-\beta_Q \hat{Q}}, \tag{A.5}$$

we can evaluate the DoS taking the inverse Laplace transform of the partition function

above:

$$\Omega(Q) = \frac{1}{2\pi i}\int_{\beta'_Q - i\infty}^{\beta'_Q + i\infty} d\beta_Q Z(\beta_Q) e^{\beta_Q Q} = \frac{1}{2\pi}\int_{-\infty}^{\infty} d\beta_Q e^{\beta'_Q Q + i\beta_Q Q + \ln Z(\beta'_Q + i\beta_Q)}. \tag{A.6}$$

Now, if $\beta_Q \neq 0$ the phase of the integrand is free to vary, leading to random phase cancellation. We must then look for $\beta_Q \approx 0$. Let us then investigate the integrand at $\beta_Q = 0$ with respect to β'_Q:

$$\partial_{\beta'_Q} e^{\beta'_Q + \ln Z(\beta'_Q)} = (Q + \partial_{\beta'_Q} \ln Z(\beta'_Q)) e^{\beta'_Q + \ln Z(\beta'_Q)}, \tag{A.7}$$

and from the result above we see that there is a maximum at

$$Q = -\partial_{\beta'_Q} \ln Z(\beta'_Q) = -\frac{\partial_{\beta'_Q} \sum_Q \Omega(Q) e^{-\beta'_Q Q}}{Z(\beta'_Q)} = \frac{\sum_Q \Omega(Q) Q e^{-\beta'_Q Q}}{Z(\beta'_Q)} = \langle \hat{Q} \rangle, \tag{A.8}$$

which fixes $\beta'_Q = \beta'_Q(Q)$, with Q given above.

We will now perform a saddle-point integration of the integral for the DoS. Expanding the exponent of the integral around $\beta_Q = 0$

$$\beta'_Q Q + i\beta_Q Q + \ln Z(\beta'_Q + i\beta_Q) \approx \beta'_Q Q + \ln Z(\beta'_Q) - \frac{1}{2}\partial^2_{\beta''_Q} \ln Z(\beta''_Q)|_{\beta'_Q} \beta_Q^2, \tag{A.9}$$

which leads to:

$$\Omega(Q) \approx \frac{e^{\beta'_Q Q + \ln Z(\beta'_Q)}}{\sqrt{2\pi \partial^2_{\beta''_Q} \ln Z(\beta''_Q)|_{\beta'_Q}}}. \tag{A.10}$$

Now:

$$\begin{aligned} \partial^2_{\beta''_Q} \ln Z(\beta''_Q)|_{\beta'_Q} =& \partial_{\beta''_Q} \frac{\sum_Q \Omega(Q) Q e^{-\beta''_Q Q}}{Z(\beta''_Q)}\bigg|_{\beta'_Q} \\ =& \left[\frac{\sum_Q \Omega(Q) Q^2 e^{-\beta''_Q Q}}{Z(\beta''_Q)} - \left(\frac{\sum_Q \Omega(Q) Q e^{-\beta''_Q Q}}{Z(\beta''_Q)}\right)^2\right]\bigg|_{\beta'_Q} \\ =& \langle Q^2 \rangle - \langle Q \rangle^2 = (\Delta Q)^2. \end{aligned} \tag{A.11}$$

Also, the entropy given in terms of the canonical ensemble (with $k_B = 1$ for simplicity)

$$S \equiv \partial_\beta (\beta \ln Z), \tag{A.12}$$

gives us

$$S(Q) = \ln Z(\beta_Q) + \beta_Q Q, \tag{A.13}$$

here we used the previous result $Q = -\partial_{\beta_Q} \ln Z(\beta_Q)$.

Using these results we can write

$$\Omega(Q) \approx \frac{e^{S(Q)}}{\sqrt{2\pi(\Delta Q)^2}}, \tag{A.14}$$

and

$$(\Delta Q)^2 \equiv \prod_{k=1}^{M} (\Delta q_k)^2. \tag{A.15}$$

Expanding the entropy around the maximal entropy configuration

$$\Omega(Q) = \prod_{k=1}^{M} \frac{\exp\left(-\frac{1}{2\alpha_k^2 N}(q_k - \overline{q}_k)^2\right)}{\sqrt{2\pi\alpha_k^2 N}}, \tag{A.16}$$

where we used that $(\Delta Q)^2 \sim \mathcal{O}(N)$, which follows from the central limit theorem, to write $(\Delta q_k)^2 = \alpha_k^2 N$, where α_k is a constant and $\overline{q}_k$ is the maximal entropy value of q_k.

Appendix B

Simulation for Spin Chain

The theory developed in this dissertation for systems with conservation laws assumes a single extensive conserved charge, and we do calculations for values of the charge at the peak in density of states (DoS). We then chose to perform simulations of such systems with spin chains with periodic boundary conditions in order to avoid finite size effects. However, the boundary conditions entail a translation symmetry which casts the Hamiltonian into a block diagonal structure (when diagonalized in momentum eigenstates), each one thermalizing within itself. Even though momentum is conserved, it is not subsystem additive, and as such does not count as a locally conserved charge. In this appendix we provide support to the assumptions made regarding the system as well as an outline how we dealt with the momentum conservation of the chain.

Firstly, we address the Gaussian density of states hypothesis. Fig. B.1 shows numerical results for the DoS for a chain of 12 spins in the regime specified in the main text. We can clearly see the Gaussian nature of the distribution, and fitting it as such allows us to identify the peak located at -0.41 ± 0.08. Analysis of the spectrum of different system sizes corroborate this result, with all peaks in the vicinity of -0.4. Moreover, in the inset of Fig. B.1 we can also see the DoS for the zero momentum sector of the spin chain, with the same characteristics.

Now, it is important to restrict simulations to a given momentum sector, as trace distances between states in different sectors are uncorrelated. In order to fix momentum states we use the shift operator,

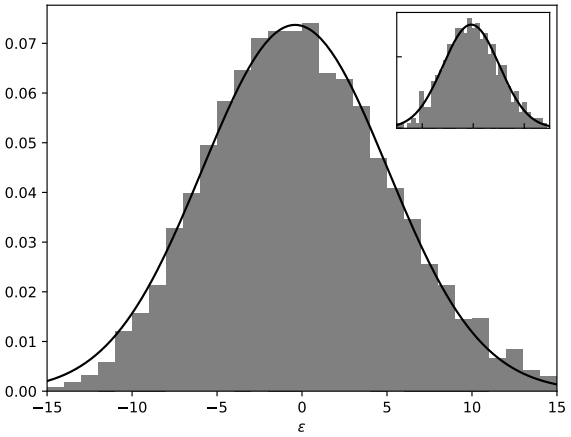

Figure B.1: Density of states for 12-spin chain. Fitted as a Gaussian the peak is observed at -0.41 ± 0.08. Inset: same analysis restricted to the zero momentum sector of the chain, and the peak is observed at -0.38 ± 0.15.

$$\mathcal{U} = \prod_{i=1}^{N-1} \frac{1}{2}\Big(\mathbb{1} + \hat{\sigma}_i^x \hat{\sigma}_{i+1}^x + \hat{\sigma}_i^y \hat{\sigma}_{i+1}^y + \hat{\sigma}_i^z \hat{\sigma}_{i+1}^z\Big), \tag{B.1}$$

which, due to the relation $\mathcal{U} = \exp(-ip)$, shares eigenstates with the momentum operator p. Diagonalizing the shift operator as $\mathcal{U} = PDP^\dagger$, the Hamiltonian for the spin chain on the eigenbasis of the shift operator $\hat{H}_0 = P^\dagger \hat{H}_S P$ is block diagonal, and properly ordering the eigenvalues of $\mathcal{U}$ in the diagonal matrix D we identify the zero momentum block as the one associated with unit eigenvalues for $\mathcal{U}$. We then diagonalize H_0 to find the energy eigenstates and write them in the usual Hilbert space basis by acting with the inverse transformation operator P on them.

Fig. B.2 shows the trace distance evaluated using the procedure outlined above to access the zero momentum sector for 10 spins. Results are for averages over trace distance between pairs of 7 states with energy closest to the density of states peak, resulting in 21 samples for averages. While this may not be a large number of samples for high precision statistics, we have to keep in mind the fact that every state selected in addition to those will have energy farther away from the DoS peak, and we develop results at the peak only. Furthermore, for this small sampling alone one can already see the signatures of the behaviour predicted by the conservation law constraints, i.e. the deviations from the structureless system trace distance curve with the predicted tendency.

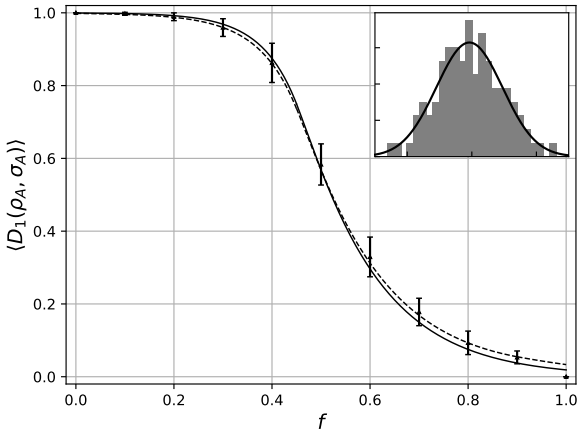

Figure B.2: Simulation of trace distance for a chain of 10 spins. Solid line shows the prediction for structureless states, given by Eq. (5.16), and dashed line is the result for systems with conservation laws, given by Eq. (5.22).

Bibliography

[1] PENINGTON, G. et al. *Replica wormholes and the black hole interior*. arXiv, 2019. Disponível em: <https://arxiv.org/abs/1911.11977>.

[2] LIU, H.; VARDHAN, S. Entanglement entropies of equilibrated pure states in quantum many-body systems and gravity. *PRX Quantum*, American Physical Society, v. 2, p. 010344, Mar 2021. Disponível em: <https://link.aps.org/doi/10.1103/PRXQuantum.2.010344>.

[3] MONTEIRO, F. et al. Quantum ergodicity in the many-body localization problem. *Phys. Rev. Lett.*, American Physical Society, v. 127, p. 030601, Jul 2021. Disponível em: <https://link.aps.org/doi/10.1103/PhysRevLett.127.030601>.

[4] ALTLAND, A.; HUSE, D. A.; MICKLITZ, T. *Maximum entropy quantum state distributions*. arXiv, 2022. Disponível em: <https://arxiv.org/abs/2203.12580>.

[5] MIRANDA, J. T. de; MICKLITZ, T. *Subsystem Trace-Distances of Random States*. arXiv, 2022. Disponível em: <https://arxiv.org/abs/2210.03213>.

[6] NANDKISHORE, R.; HUSE, D. A. Many-body localization and thermalization in quantum statistical mechanics. *Annual Review of Condensed Matter Physics*, v. 6, n. 1, p. 15–38, 2015. Disponível em: <https://doi.org/10.1146/annurev-conmatphys-031214-014726>.

[7] PAGE, D. N. Average entropy of a subsystem. *Phys. Rev. Lett.*, American Physical Society, v. 71, p. 1291–1294, Aug 1993. Disponível em: <https://link.aps.org/doi/10.1103/PhysRevLett.71.1291>.

[8] KUDLER-FLAM, J. Relative entropy of random states and black holes. *Phys. Rev. Lett.*, American Physical Society, v. 126, p. 171603, Apr 2021. Disponível em: <https://link.aps.org/doi/10.1103/PhysRevLett.126.171603>.

[9] KUDLER-FLAM, J.; NAROVLANSKY, V.; RYU, S. Distinguishing random and black hole microstates. *PRX Quantum*, American Physical Society, v. 2, p. 040340, Nov 2021. Disponível em: <https://link.aps.org/doi/10.1103/PRXQuantum.2.040340>.

[10] SACHDEV, S.; YE, J. Gapless spin-fluid ground state in a random quantum heisenberg magnet. *Phys. Rev. Lett.*, American Physical Society, v. 70, p. 3339–3342, May 1993. Disponível em: <https://link.aps.org/doi/10.1103/PhysRevLett.70.3339>.

[11] A. Kitaev, http://online.kitp.ucsb.edu/online/ entangled15/kitaev/ .... /kitaev2/ (Talks at KITP on April 7th and May 27th 2015).

[12] KIM, H.; HUSE, D. A. Ballistic spreading of entanglement in a diffusive nonintegrable system. *Phys. Rev. Lett.*, American Physical Society, v. 111, p. 127205, Sep 2013. Disponível em: <https://link.aps.org/doi/10.1103/PhysRevLett.111.127205>.

[13] KIM, H.; IKEDA, T. N.; HUSE, D. A. Testing whether all eigenstates obey the eigenstate thermalization hypothesis. *Phys. Rev. E*, American Physical Society, v. 90, p. 052105, Nov 2014. Disponível em: <https://link.aps.org/doi/10.1103/PhysRevE.90.052105>.

[14] ZHANG, L.; KIM, H.; HUSE, D. A. Thermalization of entanglement. *Phys. Rev. E*, American Physical Society, v. 91, p. 062128, Jun 2015. Disponível em: <https://link.aps.org/doi/10.1103/PhysRevE.91.062128>.

[15] DYMARSKY, A.; LASHKARI, N.; LIU, H. Subsystem eigenstate thermalization hypothesis. *Phys. Rev. E*, American Physical Society, v. 97, p. 012140, Jan 2018. Disponível em: <https://link.aps.org/doi/10.1103/PhysRevE.97.012140>.

[16] WIGNER, E. P. Characteristic vectors of bordered matrices with infinite dimensions. *Annals of Mathematics*, Annals of Mathematics, v. 62, n. 3, p. 548–564, 1955. ISSN 0003486X. Disponível em: <http://www.jstor.org/stable/1970079>.

[17] WIGNER, E. P. Characteristics vectors of bordered matrices with infinite dimensions ii. *Annals of Mathematics*, Annals of Mathematics, v. 65, n. 2, p. 203–207, 1957. ISSN 0003486X. Disponível em: <http://www.jstor.org/stable/1969956>.

[18] WIGNER, E. P. On the distribution of the roots of certain symmetric matrices. *Annals of Mathematics*, Annals of Mathematics, v. 67, n. 2, p. 325–327, 1958. ISSN 0003486X. Disponível em: <http://www.jstor.org/stable/1970008>.

[19] D'ALESSIO, L. et al. From quantum chaos and eigenstate thermalization to statistical mechanics and thermodynamics. *Advances in Physics*, Taylor & Francis, v. 65, n. 3, p. 239–362, 2016. Disponível em: <https://doi.org/10.1080/00018732.2016.1198134>.

[20] HAAKE SVEN GNUTZMANN, M. K. F. Quantum signatures of chaos. Springer Cham, 2018. Disponível em: <https://doi.org/10.1007/978-3-319-97580-1>.

[21] NIELSEN, M. A.; CHUANG, I. L. *Quantum Computation and Quantum Information: 10th Anniversary Edition*. [S.l.]: Cambridge University Press, 2011. ISBN 9781107002173.

[22] BAE, J.; KWEK, L.-C. Quantum state discrimination and its applications. *Journal of Physics A: Mathematical and Theoretical*, IOP Publishing, v. 48, n. 8, p. 083001, jan 2015. Disponível em: <https://doi.org/10.1088/1751-8113/48/8/083001>.

[23] OHYA, M.; PETZ, D. *Quantum Entropy and Its Use*. Springer Berlin Heidelberg, 2004. (Theoretical and Mathematical Physics). ISBN 9783540208068. Disponível em: <https://books.google.com.br/books?id=r2ullNVyESQC>.

[24] WILDE, M. M. *Quantum Information Theory*. [S.l.]: Cambridge University Press, 2013.

[25] KREWERAS, G. Sur les partitions non croisees d'un cycle. *Discrete Mathematics*, v. 1, n. 4, p. 333–350, 1972. ISSN 0012-365X. Disponível em: <https://www.sciencedirect.com/science/article/pii/0012365X72900416>.

[26] SIMION, R. Noncrossing partitions. *Discrete Mathematics*, v. 217, n. 1, p. 367–409, 2000. ISSN 0012-365X. Disponível em: <https://www.sciencedirect.com/science/article/pii/S0012365X99002733>.

[27] LASHKARI, N. Modular hamiltonian for excited states in conformal field theory. *Phys. Rev. Lett.*, American Physical Society, v. 117, p. 041601, Jul 2016. Disponível em: <https://link.aps.org/doi/10.1103/PhysRevLett.117.041601>.

[28] ZHANG, J.; RUGGIERO, P.; CALABRESE, P. Subsystem trace distance in quantum field theory. *Phys. Rev. Lett.*, American Physical Society, v. 122, p. 141602, Apr 2019. Disponível em: <https://link.aps.org/doi/10.1103/PhysRevLett.122.141602>.

[29] PUCHAŁA, Z.; PAWELA, Ł.; ŻYCZKOWSKI, K. Distinguishability of generic quantum states. *Phys. Rev. A*, American Physical Society, v. 93, p. 062112, Jun 2016. Disponível em: <https://link.aps.org/doi/10.1103/PhysRevA.93.062112>.